THE ASTROPHYSICAL JOURNAL SUPPLEMENT SERIES, 122:29–50, 1999 May

THE MOLONGLO REFERENCE CATALOG 1 Jy RADIO SOURCE SURVEY. IV. OPTICAL SPECTROSCOPY OF A COMPLETE QUASAR SAMPLE

JOANNE C. BAKER
School of Physics, University of Sydney, NSW 2006, Australia and MRAO, Cavendish Laboratory, Madingley Road, Cambridge CB3 0HE, UK; jcb@mrao.cam.ac.uk

RICHARD W. HUNSTEAD
School of Physics, University of Sydney, NSW 2006, Australia

AND

VIJAY K. KAPAHI AND C. R. SUBRAHMANYA
National Centre for Radio Astrophysics, TIFR, Pune University Campus, Ganeshkhind, Pune 411007, India
Received 1998 May 7; accepted 1998 December 3

ABSTRACT

Optical spectroscopic data are presented here for quasars from the Molonglo Quasar Sample (MQS), which forms part of a complete survey of 1 Jy radio sources from the Molonglo Reference Catalog. The combination of low-frequency selection and complete identifications means that the MQS is relatively free from the orientation biases that affect most other quasar samples. To date, the sample includes 105 quasars and six BL Lac objects, 106 of which have now been confirmed spectroscopically. This paper presents a homogenous set of low-resolution optical spectra for 79 MQS quasars, the majority of which have been obtained at the Anglo-Australian Telescope. Full observational details are given and redshifts, continuum, and emission-line data tabulated for all confirmed quasars.

Subject headings: galaxies: active — quasars: emission lines — quasars: general — surveys

1. INTRODUCTION

It has been widely claimed that orientation plays a crucial role in the classification of active galactic nuclei (AGNs), acting to increase the observed diversity. This idea has been formulated into the "unified schemes" for AGNs (reviewed by Antonucci 1993), which attempt to reduce the diversity by finding evidence that some classes of AGN are identical except for viewing direction. One of the most successful applications has been the description of core- and lobe-dominated quasars as being identical except for radio-jet orientation. In this picture, core-dominated quasars are simply foreshortened lobe-dominated quasars viewed with Doppler-boosted cores (Orr & Browne 1982; Kapahi & Saikia 1982).

Implicit in the unified schemes for AGNs is the presence of anisotropic emission in many wavebands. As well as predicting orientation dependencies, anisotropic emission also implies that selection biases must affect all samples of AGNs to some degree; brighter and therefore preferentially oriented AGNs will tend to be favored. To overcome or compensate for such selection effects, samples should be arguably well defined (e.g., Hewett & Foltz 1994) and if possible selected by some *isotropic* property, such as extended radio emission. However, additional biases can be introduced by imposing inappropriate flux limits at other wavelengths, most commonly the optical. For example, the paucity of lobe-dominated quasars in the B2 sample compared with the 3CR (de Ruiter et al. 1986) has been attributed to missing faint optical counterparts below the Palomar Sky Survey plate limit (Kapahi & Shastri 1987). This follows if the optical continuum in quasars is aspect dependent.

Many observations have pointed to the optical continuum emission in quasars being highly anisotropic (Browne & Wright 1985; Jackson & Browne 1989). However, none of these early studies had been able to disentangle the aspect dependence from the effects of sample selection. Indeed, with the exception of the 3CR (Laing, Riley, & Longair 1983), all previous studies have used data from samples with unknown biases and selection effects. To rectify this, and also to quantify the effects of imposing optical constraints on other samples, we have defined a new sample of southern, radio-loud quasars, the Molonglo Quasar Sample (MQS), defined below. The MQS has been defined using minimal selection criteria; it includes all radio-loud quasars in a region of sky down to a radio flux density limit of 0.95 Jy at 408 MHz. Sources were drawn initially from the Molonglo Reference Catalog (MRC; Large et al. 1981). The quasar identifications have proceeded largely in parallel with identifications of all the other sources in the same sky strip, which has ensured that no quasars have remained unidentified because they are optically faint, for example, or because they have large radio-optical positional offsets as a result of asymmetric radio structure.

In this paper, optical spectroscopic data are presented for the MQS, including tabulated redshifts, continuum and emission-line data. Optical spectra are shown here for 79 MQS quasars; spectra for the remaining quasars will be published elsewhere. This paper is the fourth in a series giving basic radio and optical data for quasars and radio galaxies from the MRC/1 Jy sample. The radio galaxy identifications are listed in Paper I (McCarthy et al. 1996), and radio images are presented in Paper II (Kapahi et al. 1998a). Radio data for the quasars are presented in Paper III (Kapahi et al. 1998b), together with a detailed description of the identification of the quasar sample. A full set of optical finding charts is included in Paper III. Other papers based on an earlier listing of the MQS have been published, including investigations into the aspect dependence of the optical continuum in the MQS by Baker & Hunstead (1995) and Baker (1997), and the X-ray properties by Baker, Hunstead, & Brinkmann (1995). Many follow-up projects are underway, including infrared spectroscopy and intermediate-resolution optical spectroscopy of high-

redshift MQS quasars (Baker & Hunstead 1996; Baker 1998).

2. THE MOLONGLO QUASAR SAMPLE

As described in a companion paper (Paper III), the selection criteria for the MQS were designed to minimize the orientation-dependent biases present in most other radio-selected samples. To achieve this, initial selection was made at low frequency where the radio emission is dominated by the steep-spectrum extended components, and complete optical identifications were then sought.

The complete flux-limited radio sample from which the quasar sample was selected consists of 557 sources with flux densities exceeding 0.95 Jy at 408 MHz in the MRC in a 10° declination strip ($-20° > \delta > -30°$), excluding those with low Galactic latitude $|b| < 20°$ and those in the R.A. range 14^h03^m–20^h20^m (due to constraints on observing time). Within this strip, sources were imaged first at 843 MHz with the Molonglo Observatory Synthesis Telescope (MOST) (Subrahmanya & Hunstead 1986) and then at higher resolution (1″) with the VLA, mostly at 5 GHz (see Paper III). The VLA snapshot images have allowed the separation of compact and extended radio components from which the core-to-lobe flux density ratios, R, have been estimated. The values of R at an emitted frequency of 10 GHz, R_{10}, are listed in Paper III for all sources except compact, steep-spectrum (CSS) sources, which we define as having radio linear sizes $l < 20$ kpc ($H_0 = 50$ km s^{-1} Mpc^{-1} and $q_0 = 0.5$ assumed throughout) and spectral indices steeper than $\alpha = 0.5$ ($S \propto \nu^{-\alpha}$) between 408 MHz and 5 GHz; see, for example, Fanti & Fanti (1994). In common with other studies, R is assumed to be an indicator of jet-axis orientation (e.g., Orr & Browne 1982). The distribution of R values for the MQS (see Baker 1997) is consistent with the sample being randomly oriented apart from an excess of core-dominated quasars, whose Doppler-enhanced emission pushes them above the radio flux limit. We note that no such bias arises in the optical because complete identifications have been made.

Optical counterparts near the radio core and/or radio centroid positions were identified first by eye (as described in Paper III) by their "stellar" appearance on the UK Schmidt IIIaJ plates, down to the limiting magnitude of $b_J \approx 22.5$ [where $b_J = B - 0.23(B-V)$, Bahcall & Soneira 1980]. Deep CCD imaging (to $r \sim 24$) of the fields of most of the 557 sources at Las Campanas, as described in Paper I, also detected a number of quasar candidates, including some close to the plate limit. Spectroscopy was then sought to confirm the identifications. The MQS comprises a total of 111 quasar candidates, of which 106 have been confirmed spectroscopically to date (including six BL Lacs, only one with a measured redshift). The acquisition and reduction of the optical spectra is described in § 3.

3. OPTICAL SPECTROSCOPY

Low-resolution optical spectra have been sought for all MQS quasar candidates with mostly the 3.9 m Anglo-Australian Telescope (AAT) and also the 4 m telescope at the Cerro Tololo Inter-American Observatory (CTIO). To date, AAT spectra have been obtained for 77 quasar candidates (plus 2 BL Lac objects). Another two quasar spectra were obtained with the ESO 3.6 m telescope (Wall & Shaver 1993, private communication). Low signal-to-noise spectra, confirming only redshifts and classifications, have been obtained at CTIO for 14 more quasars but were inadequate for accurate emission-line measurements and have not been included in this compilation. Further spectroscopy is being sought. Another five candidates await spectroscopic confirmation, including two lobe-dominated and three CSS targets. Seven more quasars have spectral data published in the literature and have not been reobserved. Data for these remaining objects will be published separately. The observations and reduction of the AAT spectra are described below.

3.1. *Journal of Observations*

The majority of spectra were obtained in three observing runs at the AAT: 1989 August 2–3, 1991 March 15–16, and 1993 June 22–23. In addition, a small number of spectra were obtained through AAT service observations and by collaborators as part of their back-up programs. Table 1 summarizes the instrumental setup and observing conditions for the AAT observations.

On the AAT, we used the RGO spectrograph at the f/8 Cassegrain focus. A dichroic beam splitter directed the red light to FORS (Faint Object Red Spectrograph) and the blue light to either the IPCS (Image Photon Counting System), or the Blue Thomson (BT) or Tektronix (Tek) CCD detectors. The spectral resolution of FORS is about 25 Å FWHM (10.1 Å per CCD pixel) over the range 5200–10,500 Å. The blue detectors were used with the 250B grating, yielding considerably higher resolution, about 3 Å pixel^{-1} or 7–8 Å FWHM, over a range extending from the atmospheric cutoff to the dichroic cutoff at 5400 Å.

3.2. *Observing Strategy*

Observations were made on dark nights with a slit typically 2″ wide and 2′ long on the sky, oriented at the parallactic angle. Differential atmospheric refraction along the slit from 3500–9000 Å ranged from less than 0.″2 for zenith distances ZD < 20° to ~2″ at ZD ~ 50°. A narrow slit was favored to optimize signal-to-noise ratios, but in cases of poor seeing (>2″) the slit width was increased to reduce slit losses (Table 1). Each quasar was observed in consecutive exposures with the object in one of two fixed positions on

TABLE 1

AAT OBSERVING LOG

Observation Date	Detectors	Average Seeing (arcsec)	Slit Width (arcsec)	Comments
1989 Aug 02	FORS+IPCS	1.0	1.0	Clear
1989 Aug 03	FORS+IPCS	2.0	1.5	Cloud
1989 Sep 26.....	FORS+IPCS	3.0	1.5	Poor
1991 Mar 15.....	FORS+IPCS	2.0	1.6	Clear
1991 Mar 16.....	FORS+IPCS	1.0	1.3	Clear
1992 Jun 04[a].....	FORS+BT	2–4	1.5	Clear
1992 Nov 29.....	FORS+TEK	2.0	2.0	Clear
1992 Nov 30.....	FORS+TEK	2.0	2.0	Clear
1993 Jun 22.....	FORS+TEK	1.5	1.7	Cloud
1993 Jun 23.....	FORS+TEK	4.5	2.0	Haze
1993 Nov 15[b].....	FORS+TEK	1.5	2.5	Mostly clear
1994 Apr 16	FORS	1.7	1.8	Clear

[a] ATAC Service.
[b] Rawlings et al.

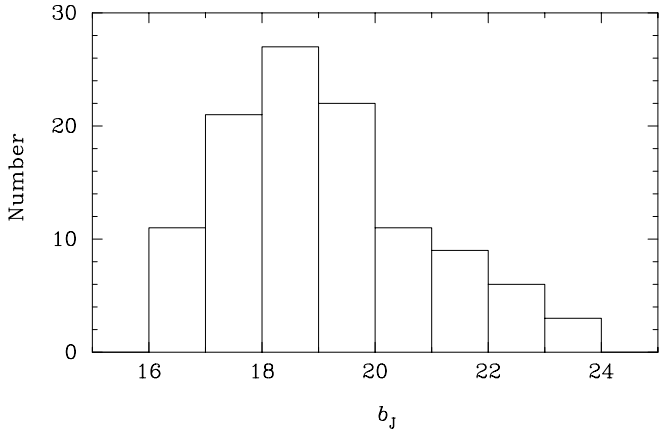

FIG. 1.—Distribution of COSMOS b_J magnitudes for the MQS. The median $b_J \approx 19$ is significantly brighter than the IIIaJ Schmidt plate limit, $b_J \approx 22.5$.

the slit. This strategy was used to optimize sky subtraction beneath the object spectrum and reduce the effect of local pixel variations. To minimize atmospheric extinction, observations were made as close to the zenith as possible. Standard stars were observed on each night at appropriate air masses to enable flux calibration and to remove atmospheric absorption features. Observations of a Cu-Ar comparison lamp were used for wavelength calibration.

3.3. *Spectral Data Reduction Method*

The AAT spectra were reduced using the FIGARO package at the University of Sydney. First, the raw CCD images were bias-subtracted and divided by a normalized flat field; this was not necessary for the IPCS data. Sky flats were used in preference to dome flats as they showed greater uniformity across the image. Cosmic-ray hits were removed interactively from regions of the CCD images close to the quasar spectrum, and then automatically over the whole image; in both cases we used interpolation from neighboring pixels. No cosmic-ray rejection was required for the IPCS data. To maximize the signal-to-noise ratio, spectra were extracted from the central few pixels of the seeing profile, consistent with the image spread due to atmospheric dispersion. Wavelength scales for both the object and sky spectra were set from the Cu-Ar lamp spectrum, achieving a typical wavelength accuracy of less than 1 Å rms.

To remove strong telluric absorption bands, the red spectra were divided by that of a smooth-spectrum star observed at a similar air mass to the quasar. The strong absorption bands were generally well subtracted, except above 9000 Å, where the residuals are magnified by the flux calibration, which is poorly constrained in this region. Corrections were also applied for atmospheric extinction in the blue in order to recover accurate continuum slopes; these corrections were mostly negligible except below about 4500 Å in a few objects observed at large air masses.

Flux calibration was applied using spectrophotometric standard stars observed on the same night as the quasars and at similar air masses. Estimated errors in flux density are typically in the range 20%–50%. The main limitations were from slit losses in poor and variable seeing, a consequence of the narrow slit used to attain high signal-to-noise ratios. The loss of narrow-line flux from extended emission regions is expected to be negligible for the majority of quasar targets (e.g., Baum et al. 1988 and Tadhunter et al. 1993).

After individually extracting and flux-calibrating the FORS and IPCS/Tek spectra, they were then joined together at wavelengths around 5400 Å. The blue spectra were rebinned first to match the resolution of FORS, improving the signal-to-noise ratio for emission-line measurements, particularly in the early IPCS data. In general, the red and blue spectra matched well in the region of the join. In cases where the match was poor the IPCS/Tek data were rescaled vertically to the FORS data. All the spectra have been shifted to a heliocentric frame of reference and the wavelength scale corrected from air to vacuum. The final wavelength coverage of the joined spectra is typically 3400–10,000 Å, with an overall spectral resolution of ~ 25 Å FWHM and average signal-to-noise ratio exceeding ten.

3.4. *Confirmation of Quasar IDs*

After spectroscopy, the original MQS candidate list yielded 100 confirmed quasars and six BL Lacs, leaving five still requiring confirmation. These five quasar candidates are retained in the list for completeness.

During the ongoing definition of the MQS, a handful of IDs were excluded at the telescope on the basis of their spectral properties. These included two targets misidentified with Galactic stars and seven objects classified after spectroscopy as narrow-line radio galaxies. The main spectral requirement for an ID to be classified as a quasar was the presence of broad emission lines. Stars were readily eliminated, and galaxies were recognized by their narrow emission lines or the 4000 Å break and other characteristic absorption features.

For the quasars comprising the MQS, the distribution of IIIaJ Schmidt-plate magnitudes b_J (drawn from the COSMOS Southern Sky Catalog) is shown in Figure 1. The distribution peaks at magnitudes significantly brighter than the plate limit, giving confidence that very few faint quasar IDs have been missed and the sample is relatively unbiased. Consistent with this, most very faint new optical counterparts from the deep CCD imaging program have turned out spectroscopically to be galaxies.

4. THE SPECTRA

Seventy-nine observed (AAT plus two ESO) spectra for the MQS are presented in Figure 2. Quasars with published optical data and not shown here have references included in Table 2. Also, spectra of BL Lacs (MRC B0118−272, MRC B1309−216 and MRC B2240−260) have been left out because data with much higher signal-to-noise ratios exist in the literature. Spectra for two borderline quasars/radio galaxies (MRC B0032−203, MRC B0201−214) are included separately in Figure 3—neither shows obvious broad lines, although the line ratios indicate higher excitation than is typical for radio galaxies. Until further investigation, it was decided that these objects should remain in the galaxy subsample.

4.1. *Comments on Individual Spectra*

MRC B0029−271.—A CSS object with an unusual optical spectrum. The peak of the strong line at about

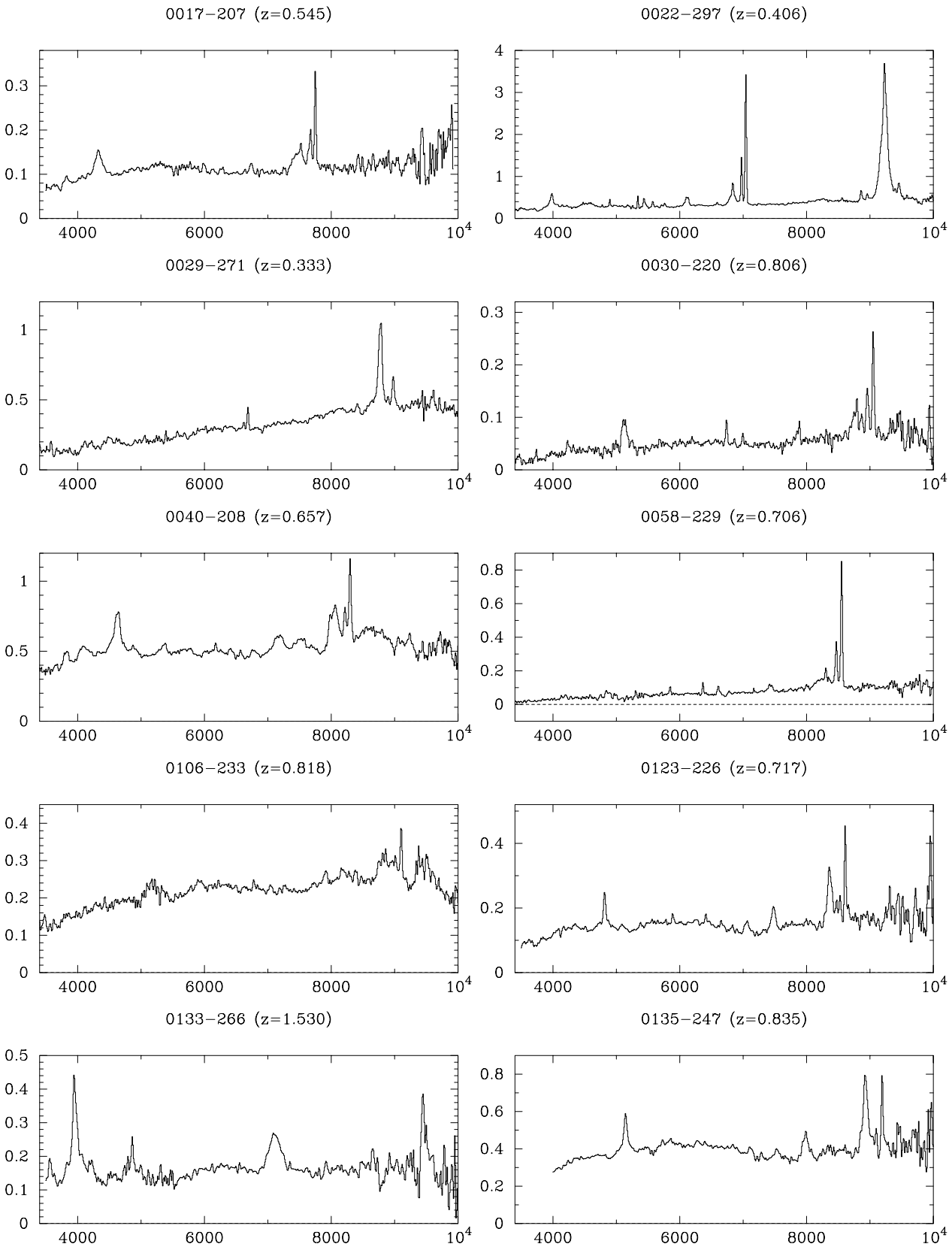

FIG. 2.—AAT optical spectra for the MQS. Flux density f_ν (mJy) is plotted as a function of wavelength (Å)

8800 Å would indicate that this line is [N II] λ6583 rather than Hα, although the broad base may contain Hα. This interpretation is supported by the presence of strong [S II] $\lambda\lambda$6717,6734 and weak or absent Hβ. The low-excitation spectrum is reminiscent of a starburst galaxy, or possibly a LINER, although [O III] is still relatively strong.

MRC B0030−220.—The Hβ and Hγ lines appear to be asymmetric with a tail to the blue.

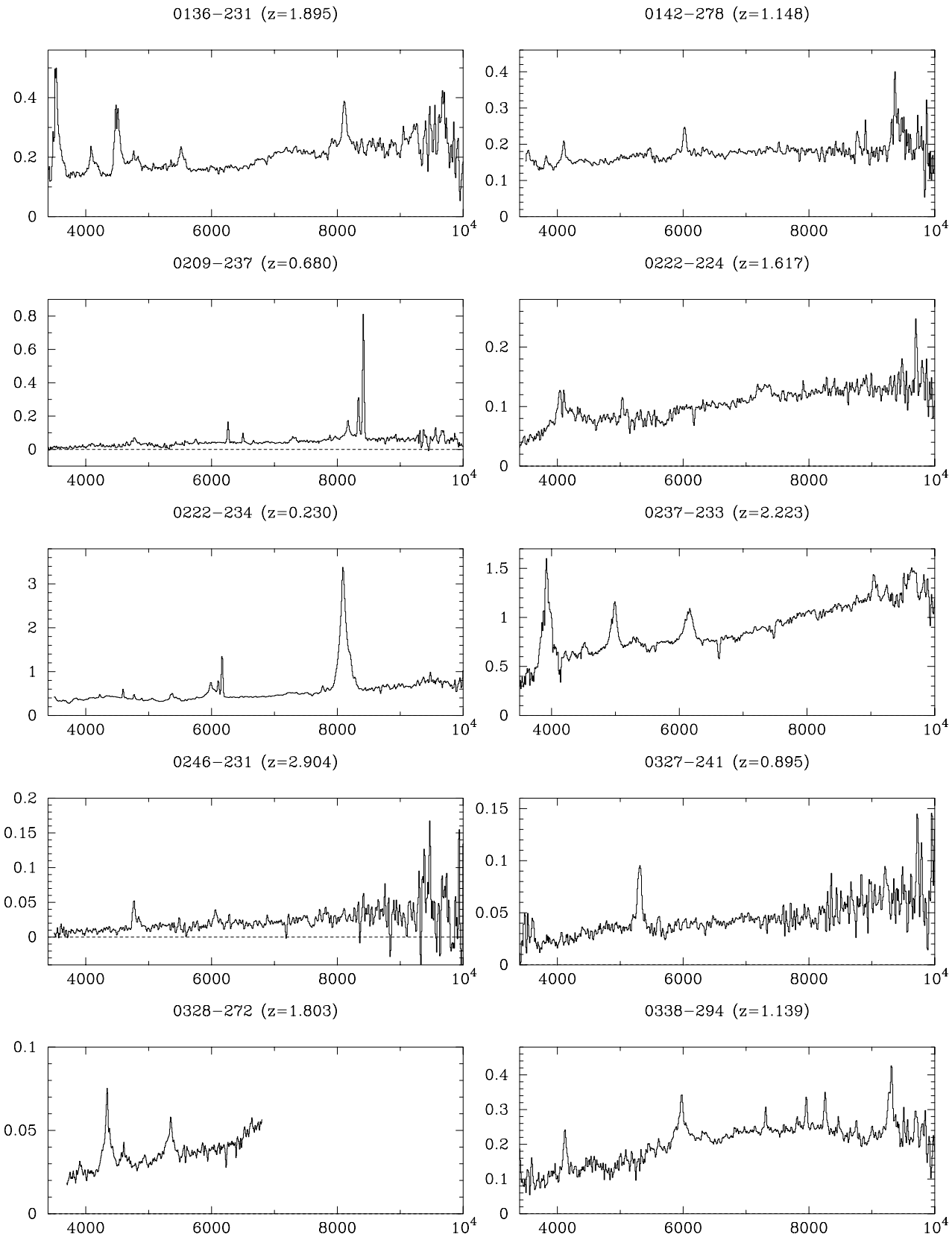

FIG. 2.—*Continued*

MRC B0106−233.—This quasar has an unusual spectrum showing copious Fe II emission and weak Mg II. [O III] is very weak.

MRC B0123−226.—The [O III] λ4959/λ5007 line ratio appears to be less than 1/3, perhaps indicating a problem with sky subtraction or possible blending with Fe II λ4924. The 3000 Å bump is prominent. The redshift was first reported by Hunstead, Murdoch, & Shobbrook (1978); an early spectrum was published by Wilkes et al. (1983).

MRC B0135−247.—This spectrum is very similar to that

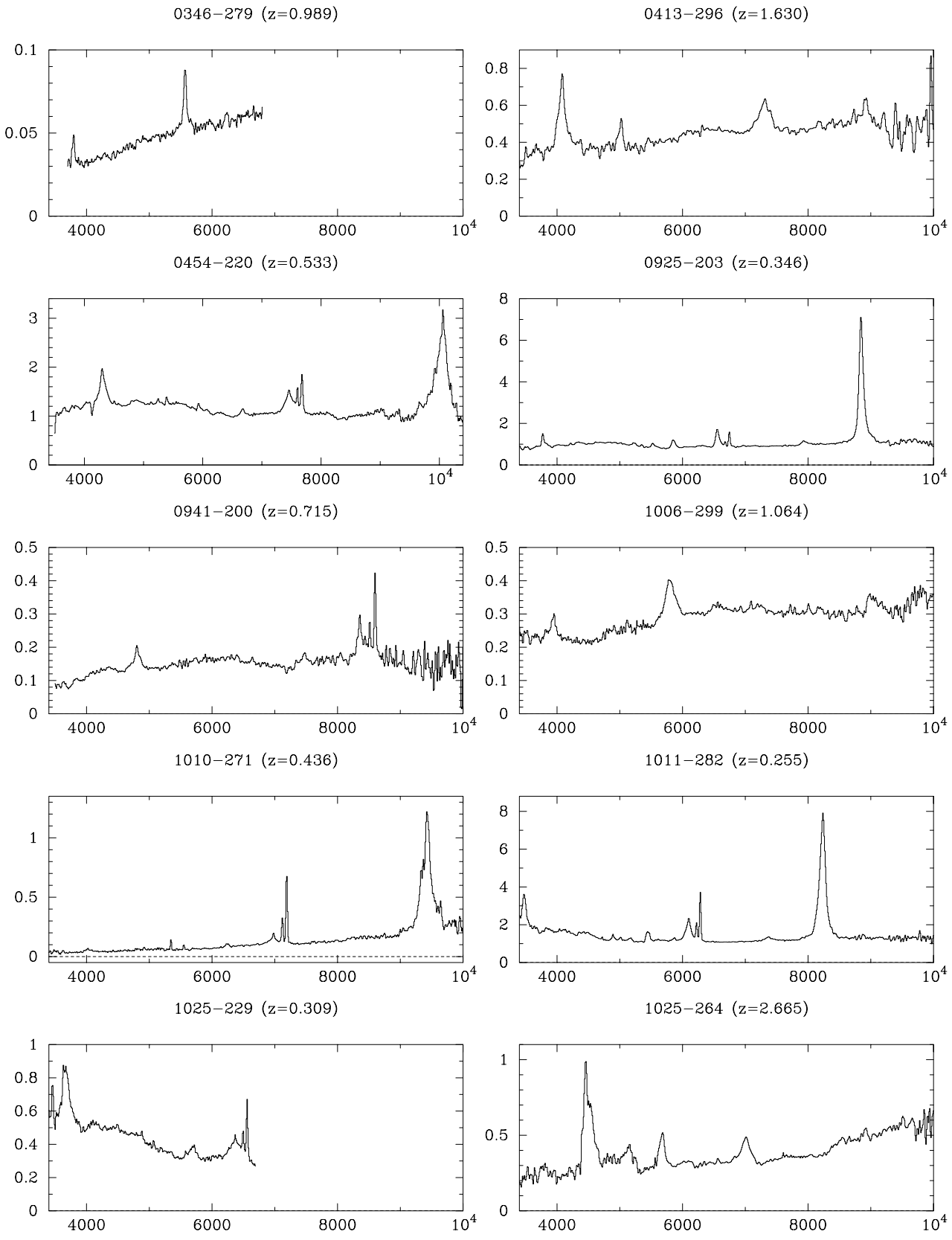

FIG. 2.—*Continued*

of MRC B0123−226. The redshift was originally determined by Jauncey et al. (1978) and spectra have been published by Wilkes et al. (1983) and Wilkes (1986). Again, [O III] λ4959 appears relatively weak, possibly as a result of blending with Fe II λ4924.

MRC B0136−231.—Lyα and C IV show absorption features just blueward of their peaks. This $z_{abs} \approx z_{em}$ absorption is also seen in the noisier spectrum published by Wilkes (1986). He II λ1640 is prominent.

MRC B0222−234.—A marked upturn is present in the

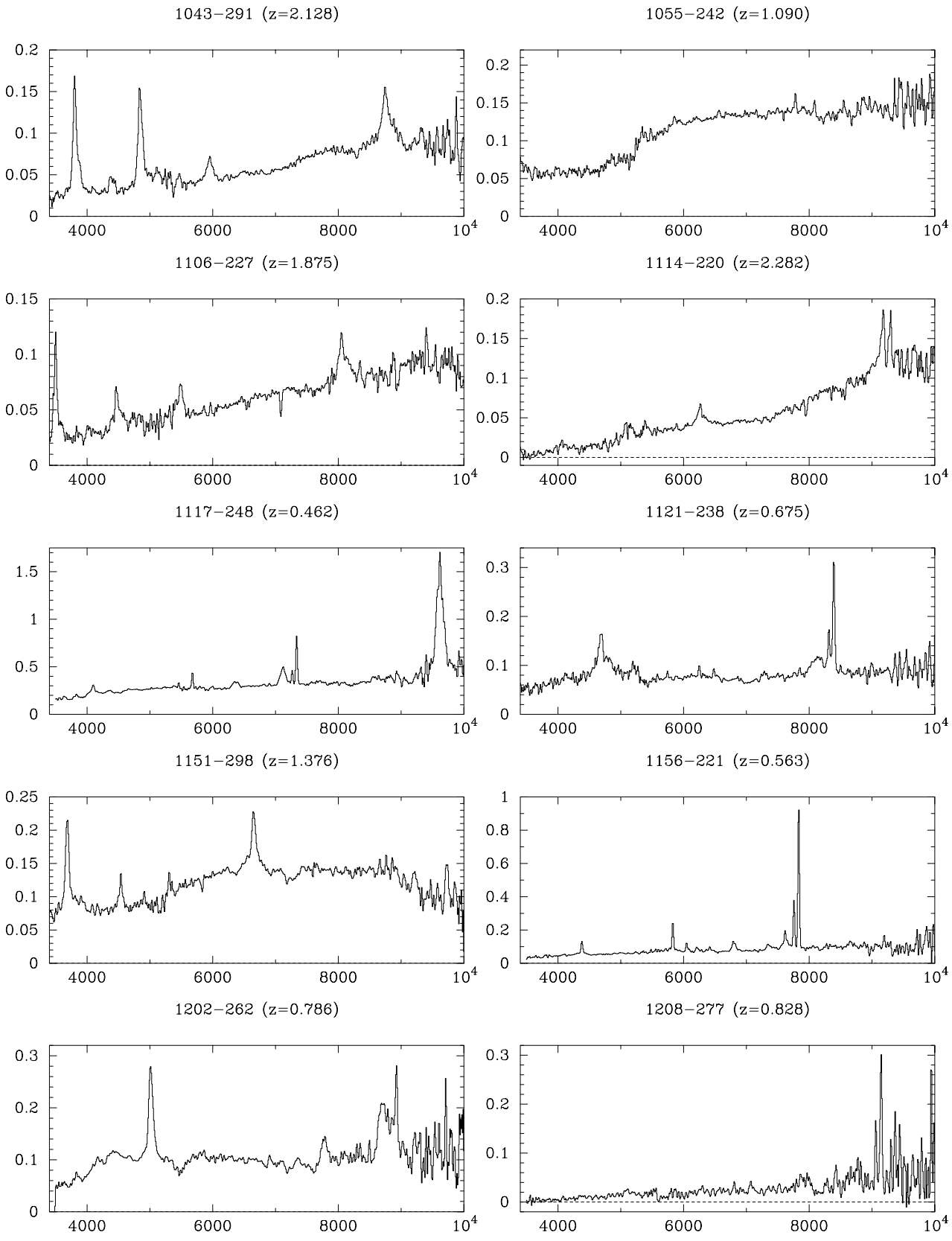

FIG. 2.—*Continued*

continuum blueward of Hγ due to the 3000 Å bump.

MRC B0222−224.—A quasar with $z_{abs} \approx z_{em}$ absorption in C IV.

MRC B0237−233.—A well-known Gigahertz peaked spectrum (GPS) quasar noted for an apparent overdensity of intervening metal absorption lines. Previous studies have been made by Wilkes et al. (1983), Wilkes (1986), Heisler, Hogan, & White (1989) and Foltz et al. (1993). Correction for atmospheric absorption distorts the AAT spectrum at wavelengths greater than 9000 Å and makes the relative flux

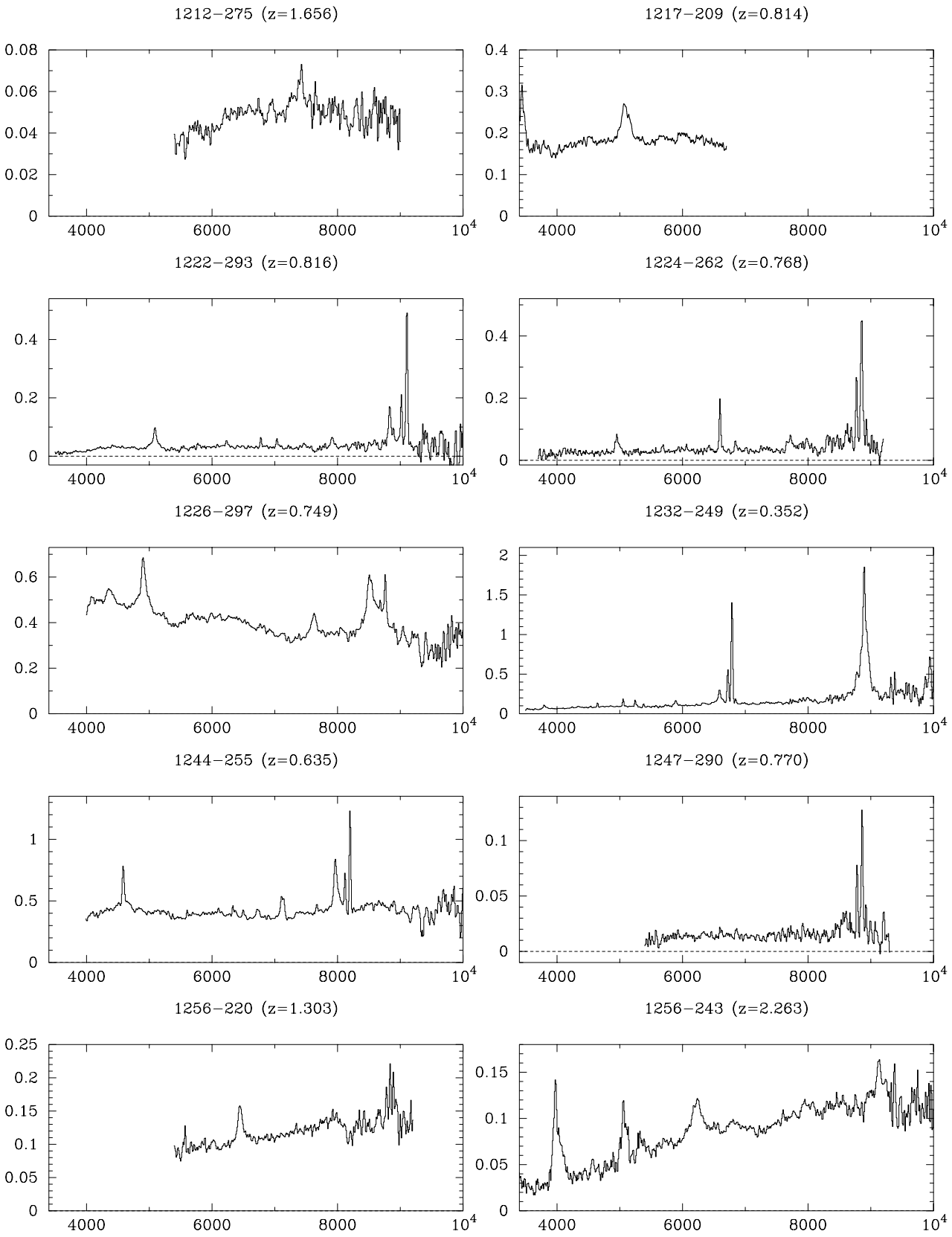

FIG. 2.—*Continued*

measurement of Mg II unreliable.

MRC B0246−231.—This is the highest redshift quasar in the MQS ($z = 2.914$). The continuum is very faint but Lyα and C IV were detected clearly.

MRC B0327−241.—The spectrum is very noisy at $\lambda > 9000$ Å making a measurement of the [O III] equivalent width impossible.

MRC B0328−272.—ESO/3.6 m spectrum, observed by

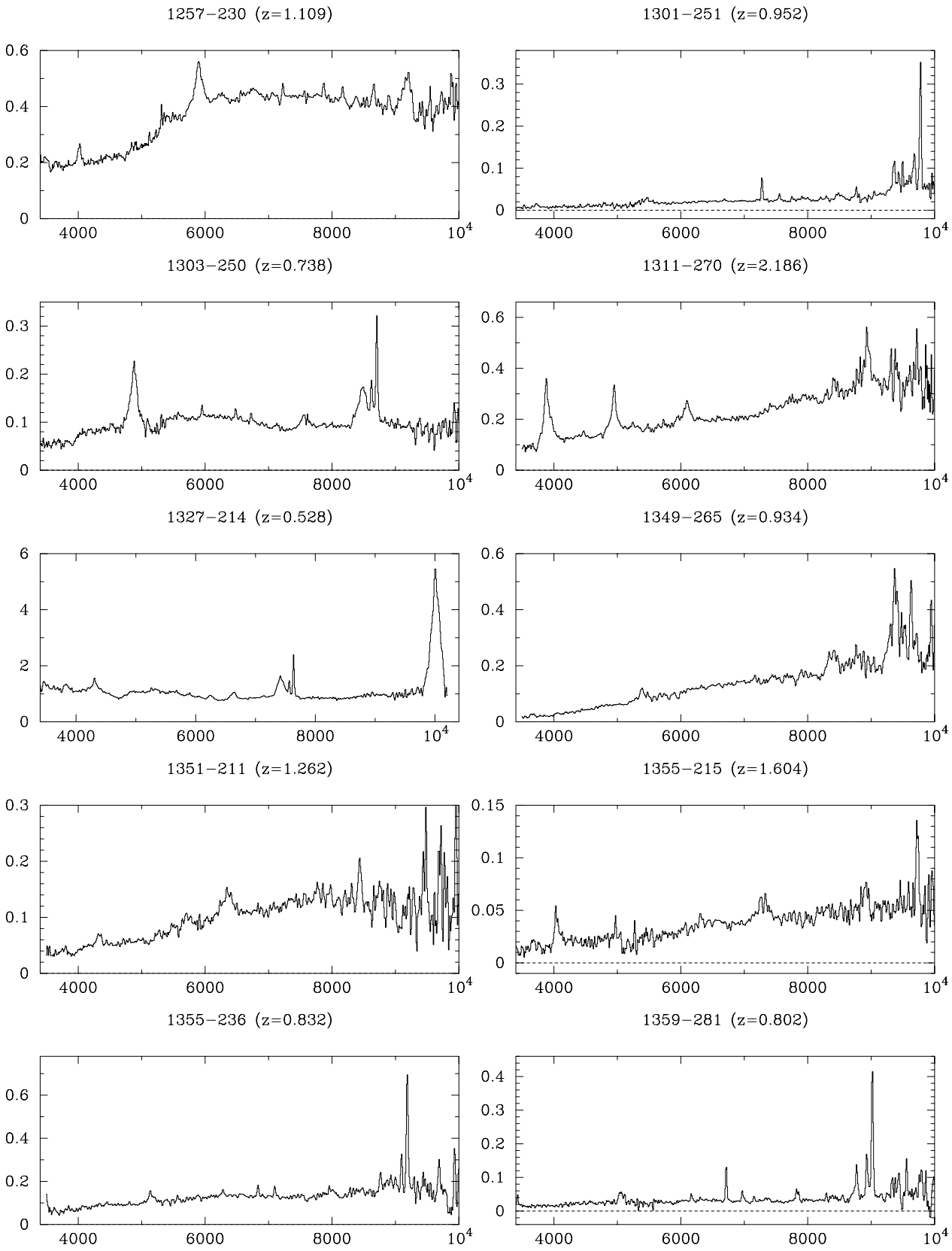

FIG. 2.—*Continued*

Wall & Shaver (1993, private communication).

MRC B0346−279.—ESO/3.6 m spectrum, observed by Wall & Shaver (1993, private communication).

MRC B0454−220.—A bright quasar showing strong broad lines. An intervening absorption system corresponding to Mg II at $z_{abs} = 0.477$ (Wright et al. 1979) is clearly visible to the blue of the Mg II emission peak; this absorption system has been well studied in the optical and UV (e.g., Bergeron & Kunth 1984; Kinney et al. 1985).

MRC B0925−203.—The blue wing of Mg II may be cut

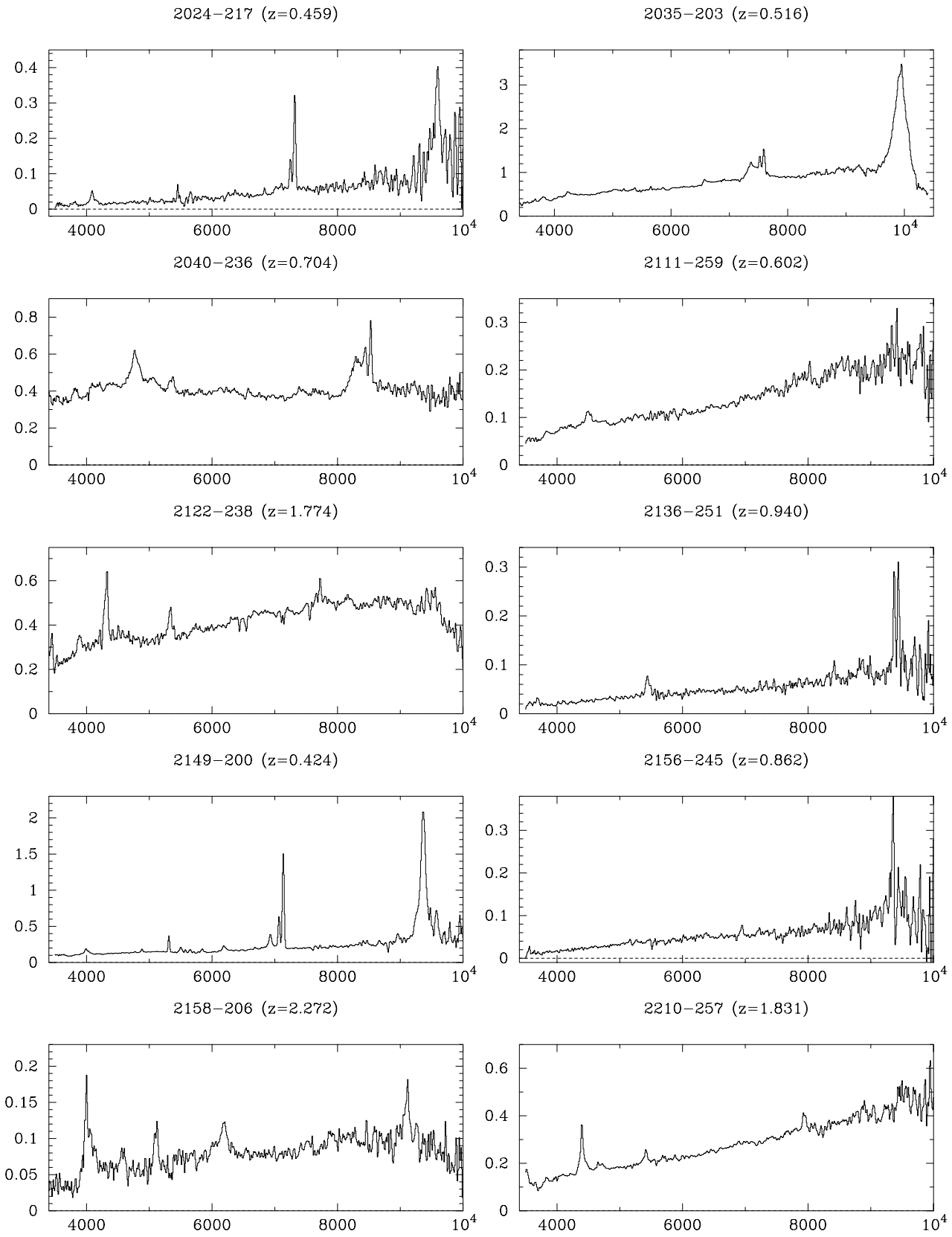

FIG. 2.—*Continued*

off by absorption, similar to that seen in MRC B1244−255.

MRC B1011−282.—This bright low-redshift quasar has been imaged extensively both in the radio and optical by Hutchings, Crampton, & Campbell (1984), Gower & Hutchings (1984), and Stockton & MacKenty (1987). It shows a nebulous optical extension to the NW, which appears to align with the stronger radio lobe. The extended nebulosity has also been studied spectroscopically by Boisson et al.

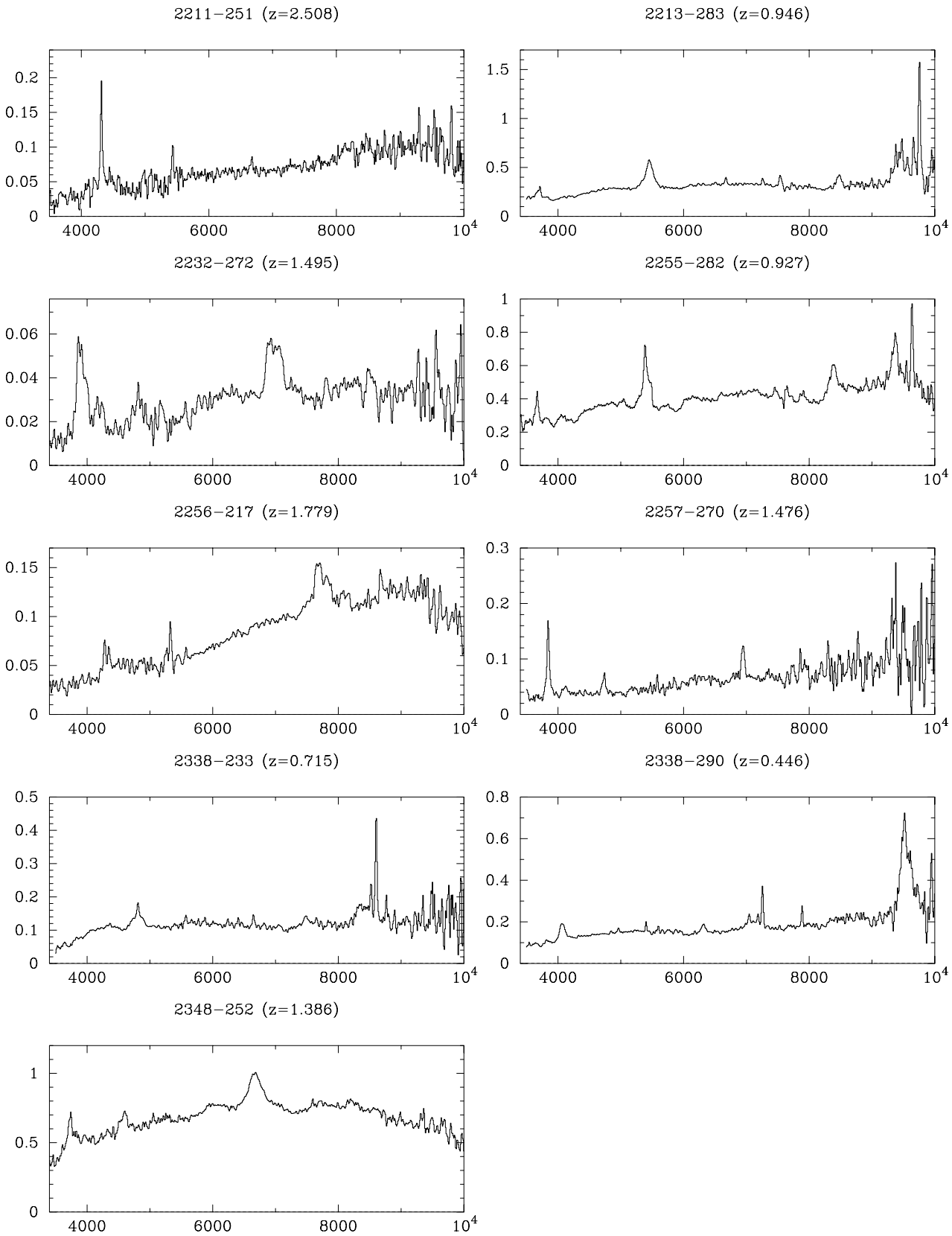

FIG. 2.—*Continued*

(1994).

MRC B1055−242.—The 3000 Å bump is very prominent in this quasar and Mg II is notably weak.

MRC B1106−227.—The Lyα and C IV emission lines show absorption just blueward of the line peaks.

MRC B1114−220.—The Lyα line appears to be heavily absorbed, and C IV appears to show absorption close to the line peak. Uncertainties in flux calibration and sky subtraction longward of 9000 Å affect the relative strength of Mg II, which may also show absorption.

TABLE 2

SPECTROSCOPY OF MOLONGLO QUASARS

MRC Quasar (1)	Date (2)	ID (3)	z (4)	α_{opt} (5)	b_J (6)	Reference (7)	Notes (8)
0017−207.....	1993 Jun 22	Q	0.545	0.38	19.3	1	S
0022−297.....	1989 Aug 03	Q	0.406	0.83	18.8	2	S
0029−271.....	1989 Aug 03	Q	0.333	1.47	19.6		SN
0030−220.....	1989 Aug 03	Q	0.806	1.54	18.9		SN
0040−208.....	1993 Nov 15	Q	0.657	0.27	16.4	3	S
0058−229.....	1989 Aug 03	Q	0.706	2.18	21.7		S
0106−233.....	1989 Aug 03	Q	0.818	0.54	20.1		SN
0111−256.....		Q	1.050	...	21.1	4	
0118−272.....	1989 Aug 02	B	...	...	17.5	5	
0123−226.....	1993 Jun 22	Q	0.717	0.58	19.9	6, 7	SN
0133−266.....	1989 Sep 26	Q	1.530	0.00	19.9		S
0135−247.....	1993 Jun 23	Q	0.835	0.31	18.9	7, 8	SN
0136−231.....	1992 Nov 30	Q	1.895	0.50	19.7	7	SN
0142−278.....	1993 Jun 23	Q	1.148	0.13	17.5	7, 9	S
0209−237.....	1989 Aug 02	Q	0.680	2.07	19.0		S
0222−234.....	1989 Aug 03	Q	0.230	1.19	18.7		SN
0222−224.....	1989 Aug 03	Q	1.617	1.13	19.1		SN
0237−233.....	1992 Nov 30	Q	2.223	0.64	16.4	7	SN
0246−231.....	1993 Jun 23	Q	2.914	1.92	21.4		SN
0301−243.....		B	...	...	16.4	4	
0315−282.....		Q	1.170	...	19.9	4	
0327−241.....	1992 Nov 29	Q	0.895	1.07	19.4	10	SN
0328−272.....	1993 Nov 14	Q	1.803	1.38	18.1	11	SN
0338−214.....		B	0.048	...	16.0	4	
0338−259.....		Q?	...	...	22.6r		
0338−294.....	1989 Aug 03	Q	1.139	0.98	18.9		S
0346−279.....	1993 Nov 14	Q	0.989	1.29	20.5	11, 12	SN
0407−226.....		Q	1.480	...	21.8r	4	
0413−210.....		Q	0.807	1.60	18.4	7	
0413−296.....	1989 Sep 26	Q	1.630	0.37	18.6		S
0418−288.....		Q	0.850	...	21.1	4	
0421−225.....		Q	0.362	...	17.5	6	
0430−278.....		Q	1.630	...	21.3	4	
0437−244.....		Q	0.84	...	17.5	4	
0439−299.....		B	...	...	20.4	4	
0447−230.....		Q	2.140	...	22.0	4	
0450−221.....		Q	0.898	1.40	17.8	1, 6	
0451−282.....		Q	2.560	1.13	17.8	7, 9	
0454−220.....	1992 Nov 29	Q	0.533	0.08	18.6	7, 13	SN
0522−215.....		Q	1.80	...	22.0	4	
0549−213.....		Q	2.245	0.00	19.1	1, 6	
0925−203.....	1992 Nov 29	Q	0.346	0.36	16.4	7	SN
0941−200.....	1993 Jun 22	Q	0.715	0.62	17.9		S
1006−299.....	1991 Mar 16	Q	1.064	0.38	18.0		S
1010−271.....	1991 Mar 16	Q	0.436	2.13	18.9		S
1011−282.....	1992 Jun 04	Q	0.255	0.22	16.3	14	SN
1017−248.....		Q?	...	...	...	4	
1019−227.....		Q	1.55	...	21.1	4	
1025−229.....	1995 Mar 31	Q	0.309	−0.71	16.7		S
1025−264.....	1991 Mar 15	Q	2.665	0.89	17.5		S
1043−291.....	1991 Mar 15	Q	2.128	1.52	18.6		S
1052−272.....		Q	1.000	...	...	4	
1055−242.....	1991 Mar 15	Q	1.090	0.95	19.9		SN
1106−227.....	1991 Mar 16	Q	1.875	1.54	20.8		SN
1114−220.....	1991 Mar 15	Q	2.282	2.77	20.2		SN
1117−248.....	1993 Jun 23	Q	0.462	0.71	17.3	7, 15	S
1121−238.....	1991 Mar 15	Q	0.675	0.40	18.6		SN
1151−298.....	1991 Mar 15	Q	1.376	0.35	18.1		SN
1156−221.....	1993 Jun 23	Q	0.563	0.92	18.6	7, 13	S
1202−262.....	1993 Jun 23	Q	0.786	1.32	19.8	13	S
1208−277.....	1993 Jun 23	Q	0.828	1.92	18.8		SN
1212−275.....	1994 Apr 16	Q	1.656	0.72	19.6		SN
1217−209.....	1995 Apr 01	Q	0.814	0.17	20.2	4	S
1222−293.....	1993 Jun 22	Q	0.816	0.66	18.5		S

TABLE 2—*Continued*

MRC Quasar (1)	Date (2)	ID (3)	z (4)	α_{opt} (5)	b_J (6)	Reference (7)	Notes (8)
1224−262.....	1995 Mar 31	Q	0.768	1.49	19.8	4	S
1226−297.....	1993 Jun 23	Q	0.749	−0.27	17.0		S
1232−249.....	1993 Jun 23	Q	0.352	1.17	17.0	7	S
1244−255.....	1993 Jun 22	Q	0.635	0.27	16.2	7, 15	SN
1247−290.....	1994 Apr 16	Q	0.770	0.43	22.1		S
1256−220.....	1994 Apr 16	Q	1.303	0.91	19.6	16	S
1256−243.....	1991 Mar 15	Q	2.263	1.41	17.6		S
1257−230.....	1991 Mar 15	Q	1.109	0.77	17.1		SN
1301−251.....	1991 Mar 16	Q	0.952	1.72	21.0		SN
1302−208.....		Q?	...	...	21.8		
1303−250.....	1991 Mar 15	Q	0.738	0.44	17.7		S
1309−216.....		B	>1.489	...	18.5	17	N
1311−270.....	1992 Jun 23	Q	2.186	1.15	19.3	12	S
1327−214.....	1992 Jun 04	Q	0.528	0.03	16.4		S
1348−289.....		Q?	...	...	19.3		
1349−265.....	1993 Jun 23	Q	0.934	2.50	18.4		S
1351−211.....	1993 Jun 22	Q	1.262	1.68	18.2	18	S
1355−215.....	1991 Mar 16	Q	1.604	1.52	19.9		S
1355−236.....	1993 Jun 22	Q	0.832	1.17	17.8		SN
1359−281.....	1991 Mar 16	Q	0.802	0.81	18.7		S
2021−208.....		Q	1.299	1.09	18.3	1, 4, 18	
2024−217.....	1993 Jun 23	Q	0.459	2.50	19.1	12	SN
2025−206.....		Q	1.400	0.74	18.7	1	
2030−230.....		Q	0.132	2.00	19.1	1, 6	
2035−203.....	1993 Nov 15	Q	0.516	1.14	16.4	3	SN
2037−234.....		Q	1.15	...	22.4	4	
2040−236.....	1993 Nov 15	Q	0.704	0.21	16.8	3	S
2059−214.....		Q?	...	...	23.1r		
2111−259.....	1993 Jun 22	Q	0.602	1.39	18.1		SN
2122−238.....	1989 Aug 02	Q	1.774	0.76	17.8		SN
2128−208.....		Q	1.610	...	20.0	4	
2136−251.....	1993 Jun 23	Q	0.940	1.97	18.1		S
2149−200.....	1993 Jun 23	Q	0.424	1.50	17.8		S
2156−245.....	1993 Jun 23	Q	0.862	2.05	20.2		SN
2158−206.....	1989 Aug 02	Q	2.272	0.63	20.1	19	SN
2210−257.....	1993 Jun 22	Q	1.831	1.10	17.9	7, 9	S
2211−251.....	1989 Aug 02	Q	2.508	1.59	19.6		S
2213−283.....	1993 Jun 23	Q	0.946	0.69	16.5		S
2227−214.....		Q	1.410	...	19.6	4	
2232−272.....	1989 Aug 02	Q	1.495	1.20	19.5		SN
2240−260.....	1989 Aug 03	B	...	...	17.9	5	
2255−282.....	1993 Nov 15	Q	0.927	0.69	16.6	3, 20	S
2256−217.....	1989 Aug 02	Q	1.779	1.31	19.9		SN
2257−270.....	1993 Jun 23	Q	1.476	1.02	18.3	7	S
2338−233.....	1993 Jun 22	Q	0.715	0.51	17.3		SN
2338−290.....	1993 Jun 22	Q	0.446	0.76	18.2		S
2348−252.....	1989 Aug 03	Q	1.386	1.38	17.3		SN

REFERENCES.—(1) Hunstead 1991, private communication; (2) Stickel et al. 1993b; (3) Rawlings 1993, private communication; (4) McCarthy 1994, private communication; (5) Stickel et al. 1993a; (6) Hunstead et al. 1978; (7) Wilkes et al. 1983, Wilkes 1986; (8) Jauncey et al. 1978; (9) Wright et al. 1983; (10) Chu et al. 1986; (11) Wall & Shaver 1993, private communication; (12) White et al. 1988; (13) Wright et al. 1979; (14) Boisson et al. 1994; (15) Savage et al. 1976; (16) Dekker & D'Odorico 1984; (17) Blades et al. 1980; (18) Murdoch et al. 1984; (19) Dunlop et al. 1989; (20) O'Dea et al. 1991.

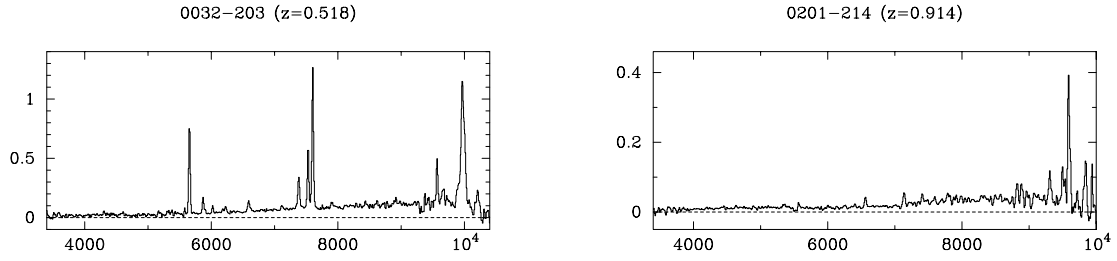

FIG. 3.—Spectra for two MRC sources that were rejected from the MQS as probable radio galaxies. Axes are f_ν (mJy) and wavelength (Å).

MRC B1121−238.—The Hβ emission line has a rounded profile with no evidence for a narrow component, while Mg II shows both a narrow and a very broad component. The possible emission feature at about 5100 Å may be accentuated by the join between the FORS and IPCS spectra.

MRC B1151−298.—The region around the spectral join at 5400 Å is noisy and so the scaling between the FORS and IPCS spectra is uncertain.

MRC B1208−277.—A faint quasar with poor signal-to-noise ratio above 9000 Å. [O III] and Hβ are discernible but the other lines are weak.

MRC B1212−275.—Only a FORS spectrum is available—the broad emission line is identified with Mg II. The measurement of α_{opt} is uncertain due to the limited wavelength coverage and presence of the 3000 Å bump.

MRC B1244−255.—Mg II shows a prominent narrow component.

MRC B1257−230.—The prominence of the 3000 Å bump makes α_{opt} uncertain.

MRC B1301−251.—The spectrum is noisy above 9000 Å, making Hβ and [O III] fluxes uncertain.

MRC B1309−216.—A BL Lac object studied by Blades, Murdoch, & Hunstead (1980); no spectrum is given here. No emission lines were found by Blades et al., but a redshift limit of $z \geq 1.49$ was set by the detection of C IV absorption lines.

MRC B1355−236.—This quasar was observed on two occasions at the AAT, showing little change apart from a possible fall in the strength of Hβ between 1991 March and 1993 June. The most recent observing date only is listed in Table 2, and the corresponding spectrum shown in Figure 2.

MRC B2024−217.—Hβ is very weak compared with Hα and appears to be very broad with no narrow component. The continuum is also very red.

MRC B2035−203.—[O III] λ5007 is affected by atmospheric *A*-band absorption.

MRC B2111−259.—The emission lines are very weak in this spectrum; the strongest line is assumed to be Mg II at $z = 0.602$. An emission feature just beyond 8000 Å is consistent with weak [O III] λ5007 at the same redshift.

MRC B2122−238.—A number of strong absorption lines are present in the spectrum; these can be identified as complexes of Fe II λλ2382,2586,2600 and Mg II λλ2796,2803 at $z_{abs} \sim 1.70$ and 1.75.

MRC B2156−245.—A quasar with a steep optical spectrum and weak emission lines. Mg II may be heavily absorbed.

MRC B2158−206.—Clearly at high-redshift ($z = 2.272$), this quasar was noted in the sample of Dunlop et al. (1989) with an incorrect redshift.

MRC B2232−272.—Mg II has a broad, flat-topped profile and C IV has an asymmetric profile, possibly due to absorption. He II λ1640 is prominent.

MRC B2256−217.—Absorption is evident at the central emission wavelength of C IV and possibly also Mg II.

MRC B2338−233.—This quasar was observed on two occasions (1989 September 26 and 1993 June 22). Hβ and [O III] were better recorded in the later spectrum shown here in Figure 2. The most recent observing date only is listed in Table 2.

MRC B2348−252.—The continuum shape appears to be dominated by the 3000 Å bump and prominent Fe II emission-line blends; α_{opt}, therefore, is uncertain.

5. SPECTROSCOPIC DATA

Table 2 lists the observational details and optical properties for the MQS, including observing dates, redshifts, optical spectral indices and IIIaJ blue magnitudes, b_J, measured by COSMOS. References are supplied for quasars with published redshifts.

5.1. *Redshifts*

Redshifts, listed in Table 2, were measured from the peaks of strong emission lines. Figure 4 shows the distribution of measured redshifts for the MQS, which span the range 0.0–3.0 (median $z \approx 1$). Redshifts have not been established for five BL Lac objects. Narrow lines were used in preference to broad lines for redshift measurements to avoid possible bias arising from systematic differences (velocity shifts ~ 1000 km s^{-1}) that have been reported between narrow and broad lines (Gaskell 1982; Tytler & Fan 1992). Such velocity shifts were seen in some MQS spectra and will be discussed in a separate paper.

5.2. *Optical Spectral Indices*

Optical spectral indices, α_{opt} ($f_\nu \propto \nu^{-\alpha}$), have been measured over the observed wavelength range 3400–10,000 Å. In practice, the observed quasar continuum rarely follows a simple power law over this range, and so large uncertainties in fitted spectral index result, of the order ± 0.2. One of the most obvious spectral features that produces a deviation from the power-law continuum is the so-called "3000 Å bump," believed to arise from blended Fe II and Balmer continuum emission over the rest frame wavelength range 2000–4000 Å (Oke, Shields, & Korykansky 1984; Wills, Netzer, & Wills 1985).

The MQS includes quasars with a wide range of optical continuum slope, $-0.3 < \alpha_{opt} < 3$ with median $\alpha_{opt} \approx 1$ (Fig. 5). Furthermore, a tail of red quasars appears in the distribution of α_{opt} in Figure 5.

In Figure 6—a plot of α_{opt} against blue magnitude, b_J—a trend is evident, despite the large scatter, for red quasars (steep α_{opt}) to be optically faint. For example, all MQS quasars with $\alpha_{opt} > 1.5$ are fainter than $b_J = 18$. The correlation in Figure 6 has a (Kendall's tau) probability of $P = 0.001$ of occurring by chance (note the correlation remains significant for core-dominated quasars alone, $P = 0.02$). The correlation may be viewed alternatively as a paucity of optically bright, red quasars in the MQS, which

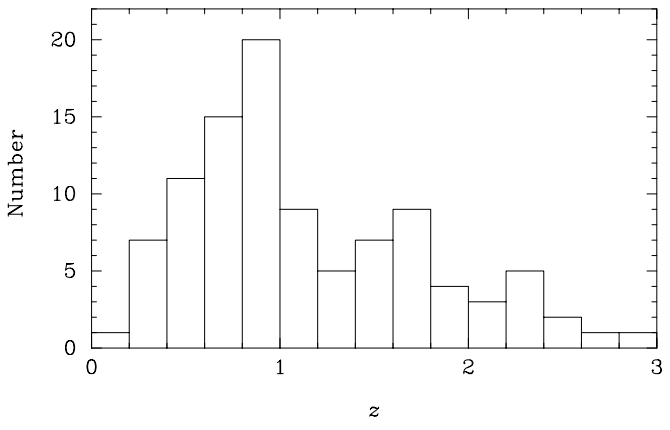

FIG. 4.—Distribution of measured redshifts for MQS quasars

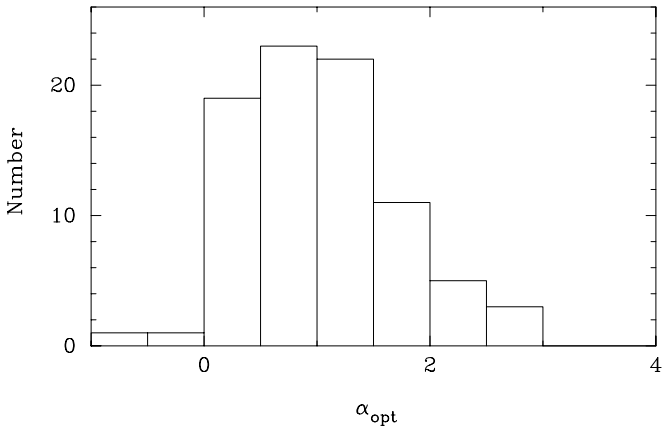

FIG. 5.—Distribution of optical spectral index, α_{opt}, for the MQS. The overall shape of the distribution is unlikely to be affected significantly by uncertainties in individual measurements of α_{opt} (20%–30%) arising from line blends and the 3000 Å bump.

is surprising since such objects are not excluded directly by our selection criteria. The fact that red MQS quasars are also optically faint may argue in favor of reddening of quasar light in these objects. Interestingly, all the quasars with $\alpha_{opt} > 1.5$ are lobe-dominated and CSS quasars, pointing to an intrinsic (possibly orientation-dependent) origin. The trend for lobe-dominated and CSS quasars to be reddened more than core-dominated quasars is confirmed by the average spectral properties of the MQS (Baker & Hunstead 1995) and is consistent with other indicators such as Balmer decrements and narrow-line equivalent widths. This issue is addressed in a paper by Baker (1997), to which the reader is referred.

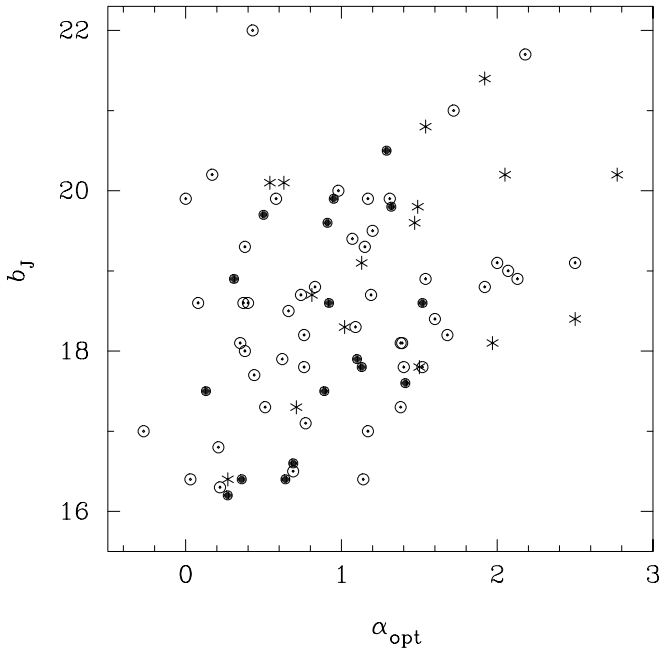

FIG. 6.—Plot of optical spectral index, α_{opt}, versus COSMOS blue magnitude, b_J. Core-dominated quasars ($R > 1$) are denoted by filled circles, lobe-dominated quasars ($R < 1$) by solar symbols, CSS by asterisks, and others by open circles.. Typical errors are 20%–30% in α_{opt}, and 0.3 mag in b_J.

5.3. *Emission-Line Fluxes*

Rest frame emission-line properties have been measured for prominent lines (see Table 3) using STARLINK DIPSO. The local continuum level was fitted in most cases by eye because of the difficulty in obtaining an acceptable fit to a power law or polynomial over the full wavelength range covered and to take account of broad emission features, such as the 3000 Å bump. Where possible, a polynomial continuum was fitted first as a guide. Errors in line fluxes were estimated empirically with repeated measurements using extreme continuum placements.

Broad Hβ and the narrow [O III] $\lambda\lambda$4959,5007 doublet were separated by integrating the [O III] emission above the red wing of Hβ and subtracting it from the total Hβ + [O III] flux. The [O III] doublet itself was not separated for flux measurements because both lines were often blended at the resolution of FORS. As the doublet ratio should be constant, combining the lines should not introduce bias. Due to the low spectral resolution no attempt has been made to separate contributions to prominent broad lines from blended species (e.g., Lyα and N V have not been separated, nor have Hα, [N II], and [S II]). It is recommended that individual spectra be viewed to judge the uncertainty of line measurements.

Rest-frame fluxes for strong lines are given in Table 3 relative to Hβ for low-redshift spectra and relative to C III] at higher redshifts where Hβ was not visible. Neither Hβ nor C III] commonly suffers absorption in quasar spectra, although at low resolution these lines may be blended with Fe II and Al III, respectively (Wills et al. 1985; Steidel & Sargent 1991). Because of the low spectral resolution, we have not attempted to separate the complex Fe II blends from the other broad-line emission in the 4500–5400 Å region. Line flux ratios are not affected by errors in the absolute flux calibration; however, uncertainties will be introduced by differences in the relative scaling of the red and blue spectra, wavelength-dependent errors in flux calibration, and extinction corrections. Errors in relative fluxes are large, estimated to be $\sim$30%, possibly greater for weak lines or in regions of poor signal-to-noise. Neighboring lines, such as Hβ and [O III] will have more accurately determined flux ratios.

Generally, the broad lines show a small dispersion in relative fluxes. On the other hand, Figure 7 shows that the ratios of [O II] and [O III] to Hβ flux span nearly four and two decades, respectively. The MQS spectra show a range of Hα/Hβ Balmer decrements from 3 to 12, suggesting that reddening is important in the MQS (see Baker 1997). Line blends may affect the fluxes of both Hα and Hβ, although not significantly for strong lines. Other diagnostic line ratios in the MQS include broad C IV/C III], which ranges between 0.8–10, and narrow [O III]/[O II], which spans 1–200.

5.4. *Equivalent Widths*

Equivalent widths, W_λ, were measured in the manner described above. Uncertainties in equivalent widths are typically 5%–15% (see Table 3) and are independent of flux calibration. The errors are slightly larger for the Mg II and [O II] lines due to uncertainty in setting the continuum level in the (rest frame) 2000–4000 Å region. Where possible, a polynomial was fitted through line-free regions of the spectrum avoiding the 3000 Å bump, and this level was used to calculate W_λ. The tabulated uncertainties in W_λ include

TABLE 3

EMISSION LINE DATA FOR MOLONGLO QUASARS

Quasar (1)	Line (2)	λ_{obs} (3)	F_{rel} (4)	W_λ (5)	Δv (6)
0017−207…	[O III]	7747	0.85	63 ± 8	u
	Hβ	7524	1.0	73 ± 16	9.5
	Hγ	6741	0.17	9.4 ± 0.4	…
	[O II]	5766	0.05	2.0 ± 0.4	u
	[Ne V]	5300	0.01	0.4 ± 0.1	u
	Mg II	4326	1.7	47 ± 3	10.2
0022−297…	Hα	9227	4.3	605 ± 57	3.5
	[O III]	7039	2.3	254 ± 18	u
	Hβ	6827	1.0	103 ± 10	4.2
	Hγ	6112	0.4	41 ± 3	…
	[O II]	5240	0.05	4 ± 2	u
	[Ne V]	4890:	0.14	9 ± 2	u
	Mg II	3980:	1.30	85 ± 24	6.6
0029−271…	[S II]	8978	…	20 ± 3	u
	[N II]	8777	…	103 ± 10	u
	[O III]	6676	…	18 ± 1.5	u
0030−220…	[O III]	9053	1.5	114 ± 6	u
	Hβ	8788	1.0n	80 ± 10	5.1
	[O II]	6725	0.35	24 ± 2	u
	[Ne V]	6191	0.06	3.0 ± 0.6	u
	Mg II	5122:	1.82	111 ± 23	7.0
0040−208…	[O III]	8289	0.6	41 ± 4	u
	Hβ	8060	1.0	74 ± 8	5.6
	Hγ	7165	0.4	25 ± 3	…
	[O II]	6172	0.06	2.7 ± 0.4	u
	Mg II	4642	1.9	48 ± 5	6.3
0058−229…	[O III]	8550	1.5	210 ± 6	u
	Hβ	8301	1.0	142 ± 16	13.0
	Hγ	7401	0.22	31 ± 3	…
	[O II]	6362	0.13	18 ± 2	u
	[Ne V]	5836	0.13	18 ± 2	u
	Mg II	4868:	0.71w	95 ± 33	8.2
0106−233…	[O III]	9102	0.25	15 ± 2	u
	Hβ	8840	1.0n	59 ± 6	13.0
	Hγ	7900	0.13	7 ± 1	…
	[O II]	6771	0.07	2.8 ± 0.4	u
	[Ne V]	6228	0.04	1.3 ± 0.3	u
	Mg II	5090:	1.06n	28 ± 2	13.5
	C III]	3432:	2.2e	39 ± 5	17.0
0123−226…	[O III]	8626	0.77	52 ± 4	u
	Hβ	8361	1.0	67 ± 18	2.8
	Hγ	7482	0.37	23 ± 3	…
	[O II]	6412	0.07	2.9 ± 0.5	u
	[Ne V]	5883	0.16	5.8 ± 0.7	u
	Mg II	4802	0.28a	17 ± 2	12.4
0133−266…	[O II]	9441:	…	…	…
	[Ne V]	8654	…	…	…
	Mg II	7087	0.55	106 ± 12	9.6
	C III]	4830	1.0n	59 ± 7	2.7
	C IV	3920	3.5	124 ± 15	13.5
0135−247…	[O III]	9182	0.40	34 ± 7	u
	Hβ	8928	1.0	79 ± 12	4.5
	Hγ	7989	0.38	24 ± 4	…
	[O II]	6836	0.005	0.20 ± 0.03	u
	[Ne V]	6278	0.016	0.5 ± 0.1	u
	Mg II	5144	0.87	22 ± 4	7.9
	C III]	[1]	…	(94)	…

TABLE 3—*Continued*

Quasar (1)	Line (2)	λ_{obs} (3)	F_{rel} (4)	W_λ (5)	Δv (6)
0136−231…	Mg II	8112	0.94	20 ± 4	2.7
	C III]	5520	1.0	13 ± 2	5.0
	C IV	4498	7.2a	60 ± 7	8.3
	Si IV	4088	3.0	21 ± 2	…
	Lyα	3519	16.2a	94 ± 9	10.9
0142−278…	[O II]	8002:	0.004	0.2 ± 0.1	u
	[Ne V]	7366:	0.011	0.5 ± 0.1	u
	Mg II	6031	0.33	11 ± 2	4.2
	C III]	4103	1.0	18 ± 1	9.1
0209−237…	[O III]	8406	2.65	294 ± 23	u
	Hβ	8163	1.0	104 ± 24	4.8
	Hγ	7290	0.38	46 ± 6	…
	[O II]	6269	0.54	72 ± 9	u
	[Ne V]	5753	0.18	24 ± 3	u
	Mg II	4765:	1.05w	210 ± 78	9.6
0222−234…	Hα	8078	5.1	560 ± 26	4.2
	[O III]	6161	0.91	76 ± 4	u
	Hβ	5977	1.0	83 ± 4	9.3
	Hγ	5364:	0.62	50 ± 4	…
	[O II]	4592	0.21	13 ± 2	u
	[Ne V]	4223	0.07	3.0 ± 0.5	u
0222−224…	[O II]	9703	0.35	16 ± 3	u
	Mg II	7277	0.79a	24 ± 5	8.8
	C III]	5031	1.0n	22 ± 1	5.8
	C IV	4080	5.22a	88 ± 15	18.6
0237−233…	Mg II	9057:	0.19e	7 ± 3	2.5
	C III]	6157	1.0	19 ± 2	7.5
	C IV	4990	1.56	19 ± 2	7.5
	Si IV	4514	0.30	4.0 ± 0.5	…
	Lyα	3921	6.1a	75 ± 7	16.0
0246−231…	C III]	7487	1.0n	12 ± 5	2.3
	C IV	6050	2.51	31 ± 7	3.7
	Si IV	5491	0.95n	14 ± 2	…
	Lyα	4771	7.5	110 ± 15	7.6
0327−241…	[O III]	9487	…	…	…
	Hβ	9207	1.0s	40 ± 6	2.7
	Hγ	8229	0.4	15 ± 2	…
	[O II]	…	<0.1	<0.8	u
	[Ne V]	6476	0.2	3 ± 1	u
	Mg II	5314	10.7w	74 ± 8	4.9
	C III]	3612	9.7e	46 ± 8	…
0328−272…	C III]	5351	1.0	31 ± 4	4.6
	C IV	4341	2.5	63 ± 7	4.9
0338−294…	Hγ	9313:	0.33	45 ± 2	…
	[O II]	7948	0.09	8.6 ± 0.7	u
	[Ne V]	7315	0.07	3.0 ± 0.3	u
	Mg II	5961	0.97	58 ± 4	10.9
	C III]	4121	1.0	45 ± 4	7.9
	C IV	3338	3.2e	200 ± 100	7.0
0346−279…	Mg II	5569	1.2	22 ± 2	2.4
	C III]	3790	1.0	15 ± 2	4.7
0413−210…	Mg II	[1]	…	(64)	…
	C III]	…	…	(38)	…
0413−296…	Mg II	7325	0.75	33 ± 2	8.6

TABLE 3—*Continued*

Quasar (1)	Line (2)	λ_{obs} (3)	F_{rel} (4)	W_λ (5)	Δv (6)
	C III]	5024	1.0	23 ± 3	6.8
	C IV	4088	3.33	48 ± 4	12.8
0450−221...	Mg II	[2]	...	(19)	...
0451−282...	C IV	[1]	...	(95)	...
	Lyα	[1]	...	(264)	...
0454−220...	Hα	10050	4.5	240 ± 26	4.8
	[O III]	7694	0.35	21 ± 2	u
	Hβ	7458	1.0	58 ± 6	6.2
	Hγ	6681	0.11	5.5 ± 0.5	...
	[O II]	5714	0.004	0.13 ± 0.07	u
	[Ne V]	5251	0.027	0.7 ± 0.07	u
	Mg II	4302	2.24a	40 ± 4	11.7
0549−213...	C III]	[2]	...	(24)	...
	C IV	[2]	...	(57)	...
	Lyα	[2]	...	(73)	...
0925−203...	Hα	8845	4.5	327 ± 28	3.2
	[O III]	6744	0.26	24 ± 2	u
	Hβ	6556	1.0	58 ± 5	2.8
	Hγ	5847	0.47	28 ± 2	...
	[O II]	5019	0.02	0.6 ± 0.1	u
	[Ne V]	4609	0.03	0.9 ± 0.1	u
	Mg II	3777	1.45a	30 ± 3	7.0
0941−200...	[O III]	8605	0.71	35 ± 3	u
	Hβ	8351	1.0	49 ± 6	5.6
	Hγ	7472	0.49	23 ± 4	...
	[O II]	6402	0.11	3.6 ± 0.6	u
	[Ne V]	5882	0.02	0.9 ± 4	u
	Mg II	4802	1.29	28 ± 3	11.0
1006−299...	Hγ	8987	0.13	8 ± 1	...
	[O II]	7720	0.02	1.0 ± 0.2	u
	[Ne V]	7094	0.025	0.9 ± 0.2	u
	Mg II	5777	1.58	41 ± 4	10.7
	C III]	3919	1.0	10 ± 1	7.1
1010−271...	Hα	9426	7.8	563 ± 58	5.8
	[O III]	7187	2.0	143 ± 15	u
	Hβ	6978	1.0	71 ± 7	8.3
	Hγ	6248	0.26	19 ± 2	...
	[O II]	5356	0.30	21 ± 2	u
	[Ne V]	4915	0.14	10 ± 1	u
	Mg II	4019	0.8	56 ± 6	11.6
1011−282...	Hα	8230	3.6	488 ± 50	3.9
	[O III]	6283	0.73	61 ± 6	u
	Hβ	6100	1.0	82 ± 8	4.8
	Hγ	5450	0.38	29 ± 3	...
	[O II]	4683	0.032	1.6 ± 0.1	u
	[Ne V]	...	<0.02	<1	u
	Mg II	3476:	2.56	35 ± 3	7.5
1025−229...	[O III]	6557	0.5	35 ± 3	u
	Hβ	6368	1.0	67 ± 7	9.6
	Hγ	5690	0.4	24 ± 2	...
	[O II]	4878	0.03	0.7 ± 0.2	u
	[Ne V]	4491	0.01	0.3 ± 0.1	u
	Mg II	3663	4.6e	66 ± 7	10.2
1025−264...	C III]	7006	1.0	25 ± 3	6.0
	C IV	5673	1.3j	24 ± 3	6.2
	Si IV	5150	1.5	17 ± 2	...

TABLE 3—*Continued*

Quasar (1)	Line (2)	λ_{obs} (3)	F_{rel} (4)	W_λ (5)	Δv (6)
	Lyα	4455	10.9	113 ± 12	12.3
1043−291...	Mg II	8751	1.17	30 ± 3	3.7
	C III]	5947	1.0	23 ± 2	4.7
	C IV	4849	5.2	73 ± 8	6.8
	Si IV	4389	1.2	19 ± 2	...
	Lyα	3802	12.4	128 ± 14	7.9
1055−242...	Hγ	9057:	0.09	2.0 ± 0.4	...
	[O II]	6556	0.20	3 ± 0.5	u
	[Ne V]	7164	0.02	0.2 ± 0.05	u
	Mg II	5849	0.6w	6 ± 2	6.1
	C III]	3991	1.0w	10 ± 1	7.5
1106−227...	Mg II	8049	0.78	36 ± 4	3.1
	C III]	5470	1.0	31 ± 4	4.7
	C IV	4456	1.20a	27 ± 3	6.4
	Si IV	4012:	0.38a	8 ± 1	...
	Lyα	3497	7.54a	96 ± 11	7.4
1114−220...	Mg II	9206	0.86a	17 ± 2	6.5
	C III]	6264	1.0a	20 ± 2	8.2
	C IV	5081	1.74a	44 ± 4	8.3
	Lyα	4061	...	...	...
1117−248...	Hα	9611	3.49	187 ± 20	5.2
	[O III]	7344	1.05	46 ± 6	u
	Hβ	7122	1.0	42 ± 5	5.6
	Hγ	6370	0.49	19 ± 2	...
	[O II]	5459	0.12	3.5 ± 0.3	u
	[Ne V]	5014	0.014	0.4 ± 0.1	u
	Mg II	4093	1.0	21 ± 4	10.0
1121−238...	[O III]	8312	1.33	80 ± 8	u
	Hβ	8120	1.0	60 ± 6	8.5
	Hγ	7285	0.19	11 ± 2	...
	[O II]	6243	0.17	7 ± 1	u
	[Ne V]	5739	0.09	1.3 ± 1	u
	Mg II	4683	4.0	80 ± 8	18.1
1151−298...	[O II]	8866	0.03	1.1 ± 0.3	u
	[Ne V]	8130	0.01	0.25 ± 0.05	u
	Mg II	6644	1.7	28 ± 3	6.1
	C III]	4535	1.0	18 ± 2	5.8
	C IV	3861	5.6	45 ± 5	8.7
1156−221...	[O III]	7842	4.0	245 ± 30	u
	Hβ	7620	1.0	61 ± 7	4.8
	Hγ	6794	0.63	37 ± 6	...
	[O II]	5830	1.0	43 ± 7	u
	[Ne V]	5343	0.06	2.3 ± 0.3	u
	Mg II	4389	1.78	68 ± 13	12.2
1202−262...	[O III]	8930	0.42s	54 ± 8	u
	Hβ	8707	1.0	130 ± 18	7.5
	Hγ	7772	0.33	37 ± 6	...
	[O II]	...	<0.01	<0.5	u
	[Ne V]	6115	0.017	1.3 ± 0.2	u
	Mg II	5010	1.27	76 ± 6	6.9
1208−277...	[O III]	9145	1.8	290 ± 50	u
	Hβ	8774:	1.0n	145 ± 50	6.5
	Hγ	7927	0.75n	109 ± 30	...
	[O II]	6815	0.13	18 ± 2	u
	[Ne V]	6296:	0.06	9 ± 1	u
	Mg II	5109:	0.28	50 ± 5	5.5

TABLE 3—*Continued*

Quasar (1)	Line (2)	λ_{obs} (3)	F_{rel} (4)	W_λ (5)	Δv (6)
1212−275…	Mg II	7406	…	8.4 ± 1.0	3.6
1217−209…	Mg II	5084	…	44 ± 4	9.7
1222−293…	[O III]	9103	1.63	411 ± 38	u
	Hβ	8827	1.0	252 ± 30	4.9
	Hγ	7916	0.27	55 ± 8	…
	[O II]	6783	0.13	18 ± 3	u
	[Ne V]	6232	0.11	13 ± 2	u
	Mg II	5088	2.14	178 ± 24	8.6
1224−262…	[O III]	8853	4.6	390 ± 50	u
	Hβ	8629	1.0s	86 ± 20	4.8
	Hγ	7724	1.0	86 ± 15	…
	[O II]	6603	1.3	111 ± 16	u
	[Ne V]	6066	0.16	10 ± 1	u
	Mg II	4963	2.0	107 ± 20	4.6
1226−297…	[O III]	8764	0.2	14 ± 3	u
	Hβ	8520	1.0	72 ± 12	8.3
	Hγ	7630	0.24	44 ± 9	…
	[O II]	6518	0.02	1.0 ± 0.3	u
	[Ne V]	5988	0.03	1.4 ± 0.3	u
	Mg II	4898	1.6	30 ± 4	9.5
1232−249…	Hα	8891	7.7	766 ± 68	4.5
	[O III]	6793	3.6	336 ± 29	u
	Hβ	6592	1.0	95 ± 14	6.5
	Hγ	5894	0.34	30 ± 4	…
	[O II]	5052	0.21	17 ± 2	u
	[Ne V]	4648	0.12	9 ± 1	u
	Mg II	3793	0.55w	46 ± 8	8.2
1244−255…	[O III]	8203	0.73	52 ± 4	u
	Hβ	7959	1.0	64 ± 6	4.6
	Hγ	7122	0.41	24 ± 2	…
	[O II]	6095	0.05	1.8 ± 0.4	u
	[Ne V]	5607	0.03	0.9 ± 0.2	u
	Mg II	4580	1.2a	24 ± 3	12.3
1247−290…	[O III]	8863	1.23	340 ± 60	u
	Hβ	8609	1.0n	240 ± 60	6.2
	Hγ	7681	0.04	8 ± 1	…
	[O II]	6600	0.006	0.7 ± 0.1	u
	[Ne V]	6061	0.02	3 ± 1	u
1256−220…	Mg II	6446	…	26 ± 3	4.7
1256−243…	Mg II	9134	0.27	14 ± 2	3.6
	C III]	6211	1.0	30 ± 3	8.2
	C IV	5053	1.21	37 ± 3	9.1
	Si IV	5065	0.3	9 ± 1	…
	Lyα	3974	5.56	161 ± 17	14.8
1257−230…	Hγ	9173	0.61	25 ± 3	…
	[O II]	7874	0.06	2.3 ± 0.5	u
	[Ne V]	7225	0.06	1.5 ± 0.5	u
	Mg II	5893	1.5	28 ± 3	8.9
	C III]	4016	1.0	12 ± 1	6.1
1301−251…	[O III]	9782	2.38s	218 ± 25	u
	Hβ	9488:	1.0s	92 ± 14	5.8
	Hγ	8482	0.34	31 ± 6	…
	[O II]	7275	0.50	42 ± 10	u
	[Ne V]	6690	0.05	4 ± 1	u
	Mg II	5465	1.09w	69 ± 10	10.7
	C III]	3722	1.61e	74 ± 18	12.9

TABLE 3—*Continued*

Quasar (1)	Line (2)	λ_{obs} (3)	F_{rel} (4)	W_λ (5)	Δv (6)
1303−250…	[O III]	8620	0.59	59 ± 5	u
	Hβ	8471	1.0	86 ± 8	8.1
	Hγ	7587	0.38	33 ± 4	…
	[O II]	6479	0.08	4.0 ± 0.5	u
	[Ne V]	5947	0.09	4.0 ± 0.5	u
	Mg II	4877	4.17	121 ± 12	9.7
1311−270…	Mg II	8933:	0.93	23 ± 4	6.2
	C III]	6094	1.0	18 ± 2	6.4
	C IV	4951	2.26	34 ± 2	11.2
	Si IV	4463	0.4	6 ± 1	…
	Lyα	3881	6.26	79 ± 4	12.8
1327−214…	Hα	10006	3.4	434 ± 38	4.8
	[O III]	7631	0.35	38 ± 3	u
	Hβ	7412	1.0	103 ± 9	6.5
	Hγ	6629	0.27	19 ± 2	…
	[O II]	5680	0.02	1.8 ± 0.3	u
	[Ne V]	5249	0.015	0.5 ± 0.1	u
	Mg II	4301	1.57	23 ± 2	12.2
1349−265…	[O III]	9622	…	…	…
	Hβ	9378	1.0s	160 ± 20	8.2
	Hγ	8383	0.26	39 ± 7	…
	[O II]	7175	0.012	1.8 ± 0.6	u
	[Ne V]	6603	0.05	0.7 ± 0.1	u
	Mg II	5385	0.26a	47 ± 7	10.4
1351−211…	[O II]	8436	0.75	23 ± 4	u
	[Ne V]	7779	0.12	6 ± 0.7	u
	Mg II	6349	2.6	44 ± 4	11.8
	C III]	4325	1.0	17 ± 5	16.7
1355−215…	[O II]	9721	0.65	20 ± 2	u
	Mg II	7307	1.48	40 ± 5	5.5
	C III]	4970	1.0	27 ± 8	10.2
	C IV	4023	5.33	71 ± 8	11.8
1355−236…	[O III]	9091	1.93	104 ± 8	u
	Hβ	8916	1.0	60 ± 12	9.7
	Hγ	7956	0.57	29 ± 10	…
	[O II]	6836	0.23	8 ± 1	u
	[Ne V]	6277	0.08	3.3 ± 0.5	u
	Mg II	5153	1.36	38 ± 7	8.9
1359−281…	[O III]	8931	3.0	273 ± 24	u
	Hβ	8767	1.0	91 ± 8	3.7
	Hγ	7824	0.34	29 ± 3	…
	[O II]	6715	0.91	74 ± 7	u
	[Ne V]	6166	0.21	15 ± 2	u
	Mg II	5050	1.90	96 ± 11	8.6
2021−208…	Mg II	6437	1.16	61 ± 7	13.2
	C III]	4390	1.0	47 ± 5	11.8
2024−217…	Hα	9590	7.47	508 ± 61	9.0
	[O III]	7323	3.12	196 ± 18	u
	Hβ	7090:	1.0	63 ± 13	8.7
	[O II]	5459	0.43	41 ± 6	u
	[Ne V]	5003	0.06	5.5 ± 0.6	u
	Mg II	4082	2.12	200 ± 44	13.0
	C III]	[3]	…	(12.5)	…
2025−206…	Mg II	6720	1.6	83 ± 35	5.7
	C III]	4582	1.0	29 ± 4	8.0
	C IV	3720	6.5	158 ± 27	16.4

TABLE 3—*Continued*

Quasar (1)	Line (2)	λ_{obs} (3)	F_{rel} (4)	W_λ (5)	Δv (6)
2030−230...	Hα	7430:	9.9	593 ± 140	7.3
	[O III]	5670:	2.45	147 ± 12	u
	Hβ	5500:	1.0	60 ± 12	4.9
	[O II]	4210:	0.93	56 ± 7	u
2035−203...	Hα	9941	4.8s	521 ± 44	7.5
	[O III]	7592	0.4	27 ± 3	u
	Hβ	7372	1.0s	66 ± 7	10.0
	Hγ	6574	0.14	9 ± 1	...
	[O II]	5651	0.04	2.4 ± 0.3	u
	Mg II	4234	0.7	29 ± 3	13.6
2040−236...	[O III]	8530	0.4	34 ± 3	u
	Hβ	8279	1.0	84 ± 8	9.3
	Hγ	7383	0.15	20 ± 2	...
	[O II]	6356	0.01	0.4 ± 0.2	u
	Mg II	4763	1.6	39 ± 4	9.4
2111−259...	Mg II	4486	...	9 ± 2	4.6
2122−238...	Mg II	7716	0.79a	8.6 ± 1.0	2.9
	C III]	5343	1.0a	7.4 ± 1.0	4.7
	C IV	4324	4.7a	26 ± 2	6.8
	Si IV	3894	2.8	10 ± 1	...
	Lyα	3377	8.8a	38 ± 2	9.6
2136−251...	[O III]	9431	...	...	...
	Hβ	8860	1.0	146 ± 54	5.2
	Hγ	8425	0.36	34 ± 7	...
	[O II]	7228	0.06	7.4 ± 0.6	u
	[Ne V]	6868	0.02	1.4 ± 0.3	u
	Mg II	5448	0.4	42 ± 15	6.9
2149−200...	Hα	9368	7.4	547 ± 72	5.3
	[O III]	7134	3.4	232 ± 7	u
	Hβ	6932	1.0	67 ± 6	3.6
	Hγ	6189	0.5	32 ± 5	...
	[O II]	5313	0.6	34 ± 3	u
	[Ne V]	4883	0.17	6.0 ± 0.6	u
	Mg II	3994	1.3	62 ± 20	13.3
2156−245...	[O III]	9368	...	...	...
	Hβ	9050	1.0s	30 ± 15	4.4
	Hγ	8096	0.4	12 ± 5	...
	[O II]	6952	0.5n	12 ± 2	u
	[Ne V]	6370	0.2	4 ± 2	u
	Mg II	5215	0.3a	15 ± 3	9.0
2158−206...	Mg II	9117	0.30	30 ± 2	3.1
	C III]	6188	1.0	60 ± 2	8.2
	C IV	5106	0.72	35 ± 4	6.4
	Si IV	4573	0.85	16 ± 2	...
	Lyα	3998	2.9	94 ± 9	11.3
2210−257...	Mg II	7938	0.5	4.4 ± 1.0	3.5
	C III]	5406	1.0	7 ± 1	5.0
	C IV	4400	5.7	33 ± 3	7.2
	Lyα	[3]	...	(120)	...
2211−251...	Mg II	9800:	...	...	...
	C III]	6675	1.0n	6.0 ± 0.5	2.7:
	C IV	5340	4.6n	27 ± 5	1.4:
	Lyα	4312	14n	65 ± 13	1.7:
2213−283...	[O III]	9749	0.78	104 ± 6	u
	Hβ	9469	1.0	133 ± 7	9.7
	Hγ	8447	0.19	23 ± 2	...
	[O II]	7263	0.05	3.8 ± 0.2	u
	[Ne V]	6668	0.04	4.2 ± 0.2	u
	Mg II	5437	1.6	83 ± 4	12.6
	C III]	3730	0.55e	20 ± 3	...
2232−272...	[O II]	9272	0.11	26 ± 7	u
	Mg II	6979	1.4a	132 ± 6	12.0
	C III]	4819	1.0	58 ± 9	12.4
	C IV	3884	5.1a	225 ± 26	17.6
2255−282...	[O III]	9632	0.6	36 ± 6	u
	Hβ	9359	1.0	59 ± 6	3.6
	Hγ	8376	0.9	43 ± 4	...
	[O II]	7176	0.01	0.4 ± 0.1	u
	Mg II	5374	1.8j	44 ± 8	6.5
	C III]	3670	1.3e	21 ± 4	6.1
2256−217...	Mg II	7757	1.7a	34 ± 5	10.4
	C III]	5363	1.0	16 ± 2	9.1
	C IV	4312	2.2n	30 ± 7	13.4
	Lyα	3347	4.7n	53 ± 4	11.6
2257−270...	[O II]	9220	0.3	15 ± 5	u
	Mg II	6952	1.0	36 ± 6	4.0
	C III]	4738	1.0	24 ± 3	4.6
	C IV	3849	5.8	128 ± 10	6.0
2338−233...	[O III]	8605	1.0	69 ± 3	u
	Hβ	8393	1.0	69 ± 6	10.8
	Hγ	7482	0.26	15 ± 2	...
	[O II]	6402	0.20	9 ± 1	u
	[Ne V]	5872	0.09	4.0 ± 0.5	u
	Mg II	4802	1.8	45 ± 3	15.6
2338−290...	Hα	9516	5.5s	270 ± 21	7.2
	[O III]	7249	0.9	35 ± 2	u
	Hβ	7037	1.0	35 ± 2	9.7
	Hγ	6317	0.56	18 ± 1	...
	[O II]	5396	0.19	4.6 ± 0.3	u
	[Ne V]	4961	0.15	5.0 ± 0.5	u
	Mg II	4071	0.31	58 ± 4	11.6
2348−252...	[O II]	8893:	0.006	0.4 ± 0.1	u
	[Ne V]	8176	0.006	0.4 ± 0.1	u
	Mg II	6676	0.41	19 ± 4	10.6
	C III]	4558	1.0	31 ± 3	13.7
	C IV	3723	1.08	24 ± 5	15.9

REFERENCES.—(1) Wilkes 1986; (2) Hunstead 1998, private communication; (3) White et al. 1988.

any differences between interpolated (polynomial fit) and local continuum flux.

Figure 8 shows the distributions of equivalent widths for the eight most prominent lines in the quasar spectrum: narrow [O III] λλ4959,5007 and [O II] λ3727, broad Hα λ6563, Hβ λ4861, Mg II λ2798, C III] λ1909, C IV λλ1549,1551, and Lyα λ1216. As expected from Figure 7, the narrow [O II] and [O III] lines show the greatest spread: four and two decades respectively. The small range of Hβ equivalent widths is notable, a consequence of the tight correlation between optical continuum and Hβ line luminosity observed in virtually all types of AGNs (Yee 1980). The distributions of W_λ in Figure 8 for the broad lines show

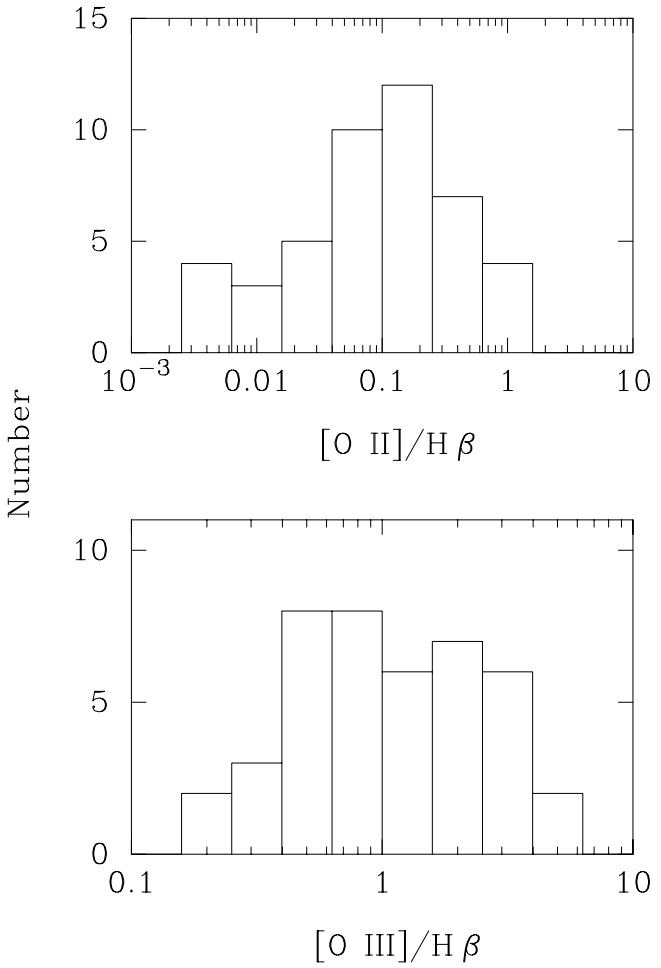

FIG. 7.—Distribution of fluxes of the narrow [O II] λ3727 line and [O III] λλ4959,5007 doublet relative to broad Hβ. Both span a large range.

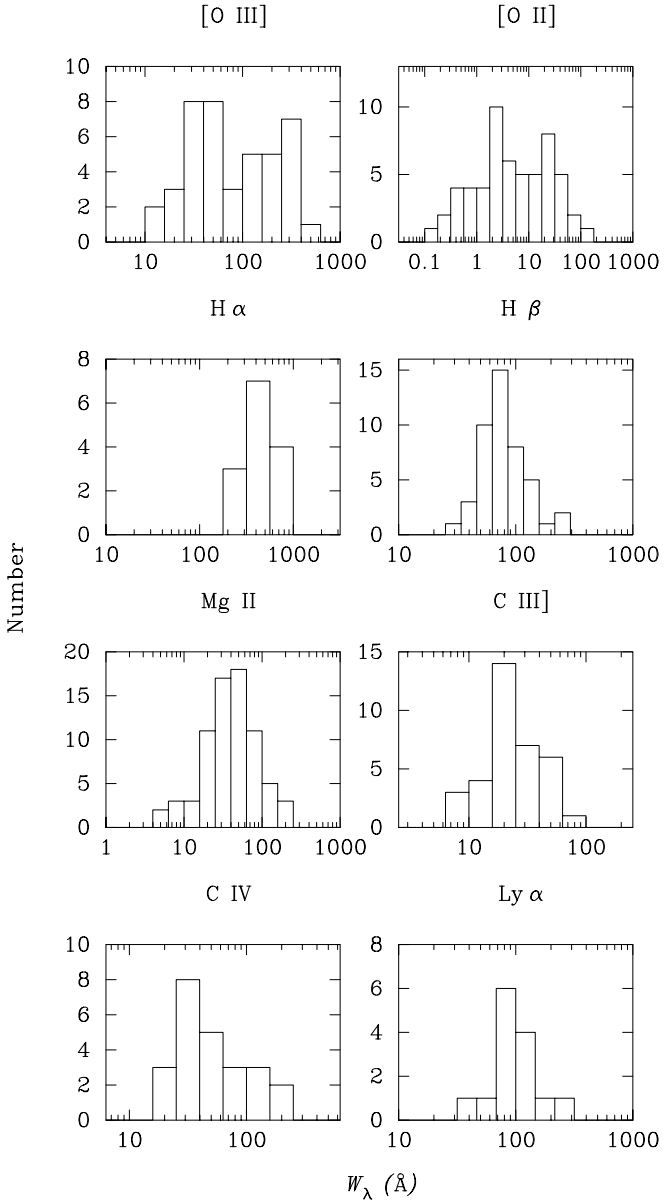

FIG. 8.—Equivalent width distributions for eight prominent emission lines; [O III] λλ4959,5007, [O II] λ3727, Hα λ6563(+[N II]), Hβ λ4861, Mg II λ2798, C III] λ1909, C IV λλ1549, 1551 and Lyα λ1216(+N V).

no prominent asymmetry, except perhaps for C IV. In general, the W_λ ranges measured for the MQS are similar to those found in other samples of both radio-loud and radio-quiet quasars (e.g., Baldwin, Wampler, & Gaskell 1989; Boroson & Green 1992; Jackson & Browne 1991).

5.5. *Emission-Line Widths*

Line widths (FWHM) have been measured for the prominent broad lines and are listed in Table 3 in km s^{-1}. No deconvolution of broad and narrow components was attempted in general; most line profiles were smooth and dominated by the broad component. In a few cases, however, with a clearly separated unresolved component sitting on top of a broad line, the width was measured from the broad component alone using eyeball deconvolution. Again, the measurement uncertainties are large, about 20%. The widths may be unreliable for emission lines with absorption occurring near the line peak. Amongst MQS quasars with $z > 1.4$, where C IV and/or Lyα is visible, absorption systems within a few thousand km s^{-1} of the line peak are seen in approximately 50% of the spectra, comparable with other studies of steep-spectrum quasars (e.g., Anderson et al. 1987) (the occurrence of associated absorption in the MQS will be addressed elsewhere; see, e.g., Baker & Hunstead 1996). Because a typical emission line profile is rarely Gaussian, as well as the possibility of absorption, observed FWHMs provide only an approximate measure of line width, particularly for strong lines with very broad wings. The line profiles and their aspect dependence will be studied in more detail in a later paper.

Figure 9 shows the distribution of velocity widths (km s^{-1}) for the four strongest broad lines. All four lines show a similar spread in line widths, from 1000–20,000 km s^{-1}. Mg II seems to have an asymmetric distribution, with a tail extending to narrower lines. Again, these values are comparable with velocity widths for quasars in other samples (e.g., Baldwin, Wampler, & Gaskell 1989).

6. NOTES TO TABLES

The spectroscopic data are presented in Tables 2 and 3. In Table 2, for each MRC quasar named (B1950 convention) the observing date is listed in column (2); the source classification (Q, quasar; Q?, likely quasar; B, BL

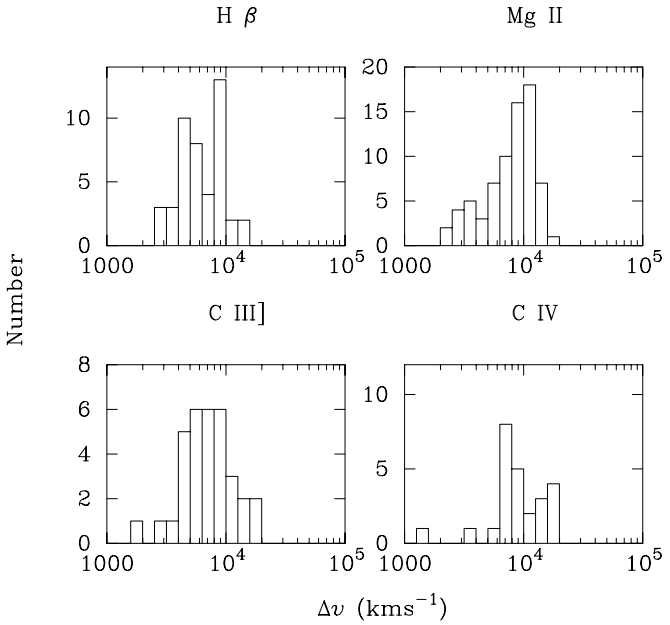

FIG. 9.—Distribution of velocity FWHMs (in km s^{-1}) for four strong broad lines: Hβ λ4861, Mg II λ2798, C III] λ1909, and C IV $\lambda\lambda$1549, 1551.

Lac) in column (3); the redshift in column (4); the optical spectral index (3000–10,000 Å observed; $S_\nu \propto \nu^{-\alpha}$) in column (5); and the COSMOS IIIaJ magnitude (r = r-band CCD magnitude) in column (6). References are supplied for individual quasars in column (7). An "N" in column (8) denotes additional notes in § 4, an "S" is given if the spectrum is shown in Figure 2.

Emission line data are presented in Table 3 for the lines Hα λ6563 (+[N II]), [O III] $\lambda\lambda$4959,5007, Hβ λ4861, Hγ λ4340 (blended with [O III] λ4363), [O II] λ3727, [Ne V] λ3426, Mg II λ2798, C III] λ1909, C IV $\lambda\lambda$1549,1551, Si IV/O IV] λ1400 (blend) and Lyα λ1216 (blended N V λ1240). The observed wavelength of the line peak is given in column (3) (only λ5007 is given for the [O III] doublet), or references given for data taken from the literature. Uncertain values are indicated with a colon throughout the table. In column (4) the ratio of the integrated line flux is given relative to broad Hβ or C III] (when no Hβ); letters show if the line measurement was affected by bad sky subtraction (s), absorption (a), noise (n), being near the edge of the spectrum (e) or a join (j), or the line is weak (w). Rest-frame equivalent widths (Å) are listed (with their measurement uncertainties) in column (5); velocity widths (FWHM) are given in column (7) ($\times 10^3$ km s^{-1}) for mostly unblended permitted lines (unresolved forbidden lines are indicated by "u").

7. CONCLUSIONS

Low-resolution optical spectroscopy has been completed for 106/111 quasars (including six BL Lacs) which comprise the MQS; 79 quasar spectra are published here (plus two borderline radio galaxy spectra). The high signal-to-noise ratios achieved, even for faint ($\sim$22 mag) targets, have allowed measurements of redshifts, spectral slopes and a wide range of emission-line properties. Redshifts for the MQS range from $z \approx 0.1$ to 3, reaching significantly higher z than the only other completely identified, low-frequency–selected sample, the 3CRR (Laing et al. 1983), which contains only one $z > 2$ quasar.

The MQS quasars show a wide range of spectral properties including a large fraction of red quasars, which are mainly lobe-dominated and CSS quasars. The emission-line properties of the MQS are in broad agreement with other studies, showing similar ranges in line widths and equivalent widths for the broad lines. The narrow oxygen lines, notably [O II], span a particularly wide range in equivalent width (see Baker 1997). Further analysis of the MQS optical data and follow-up observations are ongoing and will be presented in forthcoming papers.

We thank the referee, Chris Impey, for his helpful comments. J. C. B. was supported for part of this work by a postgraduate scholarship from the Special Research Centre for Theoretical Astrophysics, University of Sydney. R. W. H. acknowledges funding from the Australian Research Council. Staff at the Anglo-Australian Telescope are thanked greatly for their support.

REFERENCES

Anderson, S. F., Weymann, R. J., Foltz, C. B., & Chaffee, F. H., Jr. 1987, AJ, 94, 278
Antonucci, R. R. J. 1993, ARA&A, 31, 473
Bahcall, J. N., & Soneira, R. M. 1980, ApJS, 44, 73
Baker, J. C. 1997, MNRAS, 286, 23
———. 1998, in Observational Cosmology with the New Radio Surveys, ed. M. N. Bremer et al. (Dordrecht: Kluwer), 285
Baker, J. C., & Hunstead, R. W. 1995, ApJ, 452, L95
———. 1996, in The Second Workshop on GPS and CSS radio sources, ed. I. Snellen et al. (Leiden: Leiden Univ.), 166
Baker, J. C., Hunstead, R. W., & Brinkmann, W. 1995, MNRAS, 277, 553
Baldwin, J. A., Wampler, E. J., & Gaskell, C. M. 1989, ApJ, 338, 630
Baum, S. A., Heckman, T., Bridle, A. H., van Breugel, W., & Miley, G. 1988, ApJS, 68, 643
Bergeron, J., & Kunth, D. 1984, MNRAS, 207, 263
Blades, J. C., Murdoch, H. S., & Hunstead, R. W. 1980, MNRAS, 191, 61
Boisson, C., Durret, F., Bergeron, J., & Petitjean, P. 1994, A&A, 285, 377
Boroson, T. A., & Green, R. F. 1992, ApJS, 80, 109
Browne, I. W. A., & Wright, A. E. 1985, MNRAS, 213, 97
Chu, Y., Zhu, X., & Butcher, H. 1986, Chin. Astron. Astrophys., 10, 196
Dekker, H., & D'Odorico, S. 1984, ESO Messenger, 37, 7
de Ruiter, H. R., Rogora, A., & Padrielli, L. 1986, in Proc. IAU Symp. 119, Quasars, ed. G. Swarup, V. K. Kapahi (Dordrecht: Reidel), 197
Dunlop, J. S., Peacock, J. A., Savage, A., Lilly, S. J., Heasley, J. N., & Simon, A. J. B. 1989, MNRAS, 238, 1171
Fanti, C., & Fanti, R. 1994, in ASP Conf. Ser. 54, The Physics Of AGNs, ed. G. V. Bicknell, M. A. Dopita, & P. J. Quinn (San Francisco: ASP), 341
Foltz, C. B., Hewett, P. C., Chaffee, F. H., & Hogan, C. J. 1993, AJ, 105, 22
Gaskell, C. M. 1982, ApJ, 263, 79
Gower, A. C., & Hutchings, J. B. 1984, AJ, 89, 1658
Heisler, J., Hogan, C. J., & White, S. D. M. 1989, ApJ, 347, 52
Hewett, P. C., & Foltz, C. B. 1994, PASP, 106, 113
Hunstead, R. W., Murdoch, H. S., & Shobbrook, R. R. 1978, MNRAS, 185, 149
Hutchings, J. B., Crampton, D., & Campbell, B. 1984, ApJ, 280, 41
Jackson, N., & Browne, I. W. A. 1989, Nature, 338, 485
———. 1991, MNRAS, 250, 422
Jauncey, D. L., Wright, A. E., Peterson, B. A., & Condon, J. J. 1978, ApJ, 219, L1
Kapahi, V. K., et al. 1998a, ApJS, 118, 275 (Paper II)
Kapahi, V. K., et al. 1998b, ApJS, 118, 327 (Paper III)
Kapahi, V. K., & Saikia, D. J. 1982, J. Astrophys. Astron., 3, 465
Kapahi, V. K., & Shastri, P. 1987, MNRAS, 224, 17P
Kinney, A. L., Huggins, P. J., Bregman, J. N., & Glassgold, A. E. 1985, ApJ, 291, 128
Laing, R. A., Riley, J. M., & Longair, M. S. 1983, MNRAS, 204, 151
Large, M. I., Mills, B. Y., Little, A. G., Crawford, D. F., & Sutton, J. M. 1981, MNRAS, 194, 693
McCarthy, P. J., Kapahi, V. K., van Breugel, W., Persson, S. E., & Athreya, R. M., & Subrahmanya, C. R. 1996, ApJS, 107, 19 (Paper I)
Murdoch, H. S., Hunstead, R. W., & White, G. L. 1984, Proc. Astron Soc. Australia, 5, 341
O'Dea, C. P., Baum, S. A., & Stanghellini, C. 1991, ApJ, 380, 66
Oke, J. B., Shields, G. A., & Korykansky, D. G. 1984, ApJ, 277, 64
Orr, M. J. L., & Browne, I. W. A. 1982, MNRAS, 200, 1067

Savage, A., Browne, I. W. A., & Bolton, J. G. 1976, MNRAS, 177, 77P
Steidel, C. C., & Sargent, W. L. W. 1991, ApJ, 382, 433
Stickel, M., Fried, J. W., & Kühr, H. 1993a, A&AS, 97, 483
———. 1993b, A&AS, 98, 393
Stockton, A., & MacKenty, J. 1987, ApJ, 316, 584
Subrahmanya, C. R., & Hunstead, R. W. 1986, A&A, 170, 27
Tadhunter, C. N., Morganti, R., di Serego Alighieri, S., Fosbury, R. A. E., & Danziger, I. J. 1993, MNRAS, 263, 999
Tytler, D., & Fan, X.-M. 1992, ApJS, 79, 1
White, G. L., Jauncey, D. L., Savage, A., Wright, A. E., Batty, M. J., Peterson, B. A., & Gulkis, S. 1988, ApJ, 327, 561
Wilkes, B. J. 1986, MNRAS, 218, 331
Wilkes, B. J., Wright, A. E., Jauncey, D. L., & Peterson, B. A. 1983, Proc Astron. Soc. Australia, 5, 2
Wills, B. J., Netzer, H., & Wills, D. 1985, ApJ, 288, 94
Wright, A. E., Peterson, B. A., Jauncey, D. L., & Condon, J. J. 1979, ApJ, 229, 73
Wright, A. E., Ables, J. G., & Allen, D. A. 1983, MNRAS, 205, 793
Yee, H. K. C. 1980, ApJ, 241, 894